To the Graduate Council:

I am submitting herewith a thesis written by Ryan Lane Holloman entitled "A Stark-Effect Modulator for CO_2 Laser Free-Space Communications." I have examined the final electronic copy of this thesis for form and content and recommend that it be accepted in partial fulfillment of the requirements for the degree of Master of Science, with a major in Physics.

Stuart Elston
Major Professor

We have read this thesis
and recommend its acceptance:

Donald Hutchinson

Robert Compton

Accepted for the Council:

Anne Mayhew
Vice Chancellor and
Dean of Graduate Studies

(Original signatures are on file with official student records)

A Stark-Effect Modulator for CO_2 Laser Free-Space Communications

A Thesis

Presented for the

Master of Science

Degree

The University of Tennessee, Knoxville

Ryan Lane Holloman

May 2005

Acknowledgments

The author would like to acknowledge Dr. Donald Hutchinson for the tremendous knowledge, guidance, and time he provided. Also acknowledged are his colleagues Dr. Roger Richards and Dr. John Simpson for their assistance. This experiment was conceived by them and without their assistance would not have been possible. The author truly appreciates their teaching and scientific inspiration.

Also, the author would like to acknowledge his committee members, Dr. Stuart Elston and Dr. Robert Compton for their time and many suggestions.

Finally, the author thanks his family for their support and love.

Abstract

A Stark-effect modulator prototype has been designed and constructed to transmit an RF signal upon an infrared carrier wave produced by a CO_2 laser. The anticipated future use of this prototype will be to integrate it into an all-weather long-wavelength infrared (LWIR) free-space communication link. This communication system is expected to be capable of operation at 2.5 Gbits/sec over a range of >6 kilometers. The Stark-effect modulator prototype is ideal to replace existing microwave and radio communication links used currently. Also, the Stark-effect modulator is a better choice than electro-optic crystal modulators and acousto-optic Bragg cell modulators because it operates at higher frequencies and is less costly.

The Stark-effect occurs when an electric field is applied to a gas molecule that has a substantial polarizability. The electric field changes the spacing of the gas molecule energy levels. The gas molecule used is deuterated ammonia (NH_2D) because it has a molecular absorption resonance near the 10.59 micron wavelength line of the CO_2 laser emission.

The modulator is a dielectric waveguide that is constructed of borosilicate glass, measuring 36-cm in length and having an inner diameter of 1.8-mm and an outer diameter of 3-mm. The modulator has been characterized successfully, with an experimental result agreeing with a predicted model. For the first time, an RF signal has been successfully applied to the Stark-effect modulator and successfully transmitted and detected by a nearby receiver.

Table of Contents

Chapter **Page**

1. **Introduction** 1
   1-1 LWIR Communication Advantages 1
   1-2 All-Weather Capabilities 2
      1-2-1 Atmospheric Absorption 3
      1-2-2 Smoke Extinction Model 6
      1-2-3 Fog Extinction Model 8
   1-3 The Thesis 8
2. **Literature Review** 11
   2-1 Microwave Spectroscopy 12
   2-2 Infrared Spectroscopy 14
   2-3 Stark-Effect Modulation 16
   2-4 Stark-Effect Modulator at ORNL 22
      2-4-1 Theory of Stark-Effect Modulator 22
      2-4-2 Experimental Results 23
3. **Research** 27
   3-1 CO_2 Laser 27
   3-2 Stark-Effect Modulator 31
      3-2-1 Molecular Gas Filling 36
      3-2-2 AC Biasing 37
   3-3 Data Addition 39
   3-4 Experimental Arrangement 41
4. **Results** 44
5. **Conclusion** 54

References 57
Appendix 60
Vita 65

List of Tables

Table **Page**

Table 1. Experimental results for percentage modulation [10].....17

List of Figures

Figure **Page**

Figure 1. Atmospheric transmission of $^{12}C^{16}O_2$ laser wavelength [6]. 4
Figure 2. Atmospheric transmission of $^{13}C^{16}O_2$-isotope wavelength [6].....5
Figure 3. Transmission of commonly used laser wavelengths through smoke [6].....7
Figure 4. Transmission of commonly used laser wavelengths through fog [6]. 9
Figure 5. The simulated transmission of NH_2D in a 30-cm cell at 2-Torr.....24
Figure 6. The simulated transmission of NH_2D in a 30-cm cell at 2-Torr with a larger applied electric field than Figure 5 25
Figure 7. The transmission (measured) signal versus applied voltage in a 20-cm long cell filled with 8-torr of NH_2D.....26
Figure 8. The RF-driven CO_2 laser used for modulation experiments [6].....28
Figure 9. On the left is the laser housing 29
Figure 10. Schematic inside the RF insulated housing 30
Figure 11. Inside the RF insulating housing 32
Figure 12. Side view of the Stark-effect modulator.....33
Figure 13. Cross section of the Stark-effect modulator 34
Figure 14. Picture of Stark-effect modulator 35
Figure 15. The NH_2D gas is formed and supplied to the modulator here.....36
Figure 16. A schematic drawing of plumbing for the gas filling apparatus. 37
Figure 17. The bridge circuit designed for an AC bias signal 38
Figure 18. The applied AC bias on the left produces the equivalent to a steady "DC" bias as shown on the right [7] 39
Figure 19. The bias and data waveforms must match in polarity to modulate correctly [7].....40
Figure 20. An electrical schematic of the modulator circuit.....41
Figure 21. A picture of the experimental arrangement 42
Figure 22. This is a schematic diagram of the experimental arrangement 43
Figure 23. Normalized Transmission vs. Applied Voltage.....45
Figure 24. The RF drive signal had 8-Vpp driven to the modulator.....47
Figure 25. This is the detected RF transmission 48
Figure 26. This shows the transmitted RF sinusoidal signal 49
Figure 27. Normalized Measured RF Signal Amplitude vs. Drive Signal 52
Figure 28. Figure of Merit vs. Pressure 53

Chapter 1:

Introduction

In the past, there has not been an extensive application for long-wavelength infrared (LWIR) communication systems. This void could be alleviated if an economical and compact source for 10-micron radiation were developed. Therefore, this thesis in collaboration with Oak Ridge National Laboratory (ORNL) is developing a LWIR free-space communication system [6], [7]. This communication system is expected to operate at 2.5 Gbits/sec over a range of >6 kilometers. A LWIR communication system is ideal to replace currently used radio and microwave communication links.

1-1 LWIR Communication Advantages

The capacity of any communication channel is proportional to the width Δf of its frequency band [12]. Even for highly monochromatic light, where $\Delta f/f_o$ is very small the bandwidth Δf can be enormous when f_o is very high. Light waves carry very high central frequencies where f_o can reach 10^{14}-Hz. However, radio and microwave systems operate at much lower central frequencies. Therefore, light waves have the capacity to carry much more information than radio and microwave systems. In fact, because radio and microwave communications involve electromagnetic waves of longer wavelength and lower frequency than laser light the theoretical information capacity of a typical light wave is around 100,000 times greater than that for a typical microwave [12].

Besides information capacity improvements, another characteristic that makes visible and infrared light ideal to replace radio and microwave systems is that it is virtually impossible to intercept. This is because laser light does not scatter as much as radio and microwave systems. This safety feature is very attractive when security of information is important.

Ten-micron radiation has been chosen because it has unique advantages. First, 10-micron radiation is considered to be eye safe. The definition of eye safe is that corneal burning may result, but there is no retinal damage. Laboratory safety glasses are the only protection required for 10-micron radiation. Second, a very compact 10-micron CO_2 laser and Stark-effect modulator has been designed. Also, recent developments of a wideband, room temperature Quantum Well Infrared Photodetector (QWIP) receiver enable this to be a truly portable LWIR communication package [6]. Finally, LWIR radiation operates very well in natural weather phenomenon. This means it has better transmission than other laser wavelengths through atmospheric conditions such as fog, clouds, and smoke.

1-2 All-Weather Capabilities

An important feature of this communication system is its all-weather capabilities. This means more radiation may be transmitted through atmospheric conditions (fog, clouds, and smoke) using long-wavelength infrared radiation than with shorter wavelength lasers that are typically used [7]. Therefore, selecting the proper laser wavelength is of great importance since absorption and scattering are wavelength dependent. A CO_2 laser has been selected for its 10-micron range; however, a

comparison between the standard $^{12}C^{16}O_2$ and $^{13}C^{16}O_2$-isotope laser is presented in section 1-2-1.

1-2-1 Atmospheric Absorption

An atmospheric absorption comparison between the standard and isotopic CO_2 laser wavelengths is made using the database, HITRAN [5]. This database shows the superiority of the $^{13}C^{16}O_2$-isotope wavelengths (~10.8-µm) versus the standard $^{12}C^{16}O_2$ laser wavelengths (~10.6-µm) for atmospheric absorption. The improved transmission for the $^{13}C^{16}O_2$ laser wavelength occurs because the atmosphere contains very little $^{13}C^{16}O_2$. The atmospheric transmissions modeled by HITRAN are represented in Figures 1 and 2 [6]. In both of these figures, the roundtrip path length is 12-km at a pressure of 1-atm and a temperature of 296-K. Figure 1 represents the atmospheric transmission using a $^{12}C^{16}O_2$ laser. Notice that most of the lines only have ~40 percent transmission. In comparison, Figure 2 shows atmospheric transmission using the $^{13}C^{16}O_2$ laser wavelength. The three laser lines shown have a transmission between 80 and 90 percent at the same conditions. The R(20) line of $^{13}C^{16}O_2$ has the best atmospheric transmission.

To further promote the 10-µm wavelength region as ideal for an all-weather communication link, a summary of some known effects upon the transmission of radiation through smoke and fog is presented [6]. In these sections the 10-µm wavelength region will be compared to other wavelengths (500-µm and 1.5-µm), which are currently popular for optical communication systems.

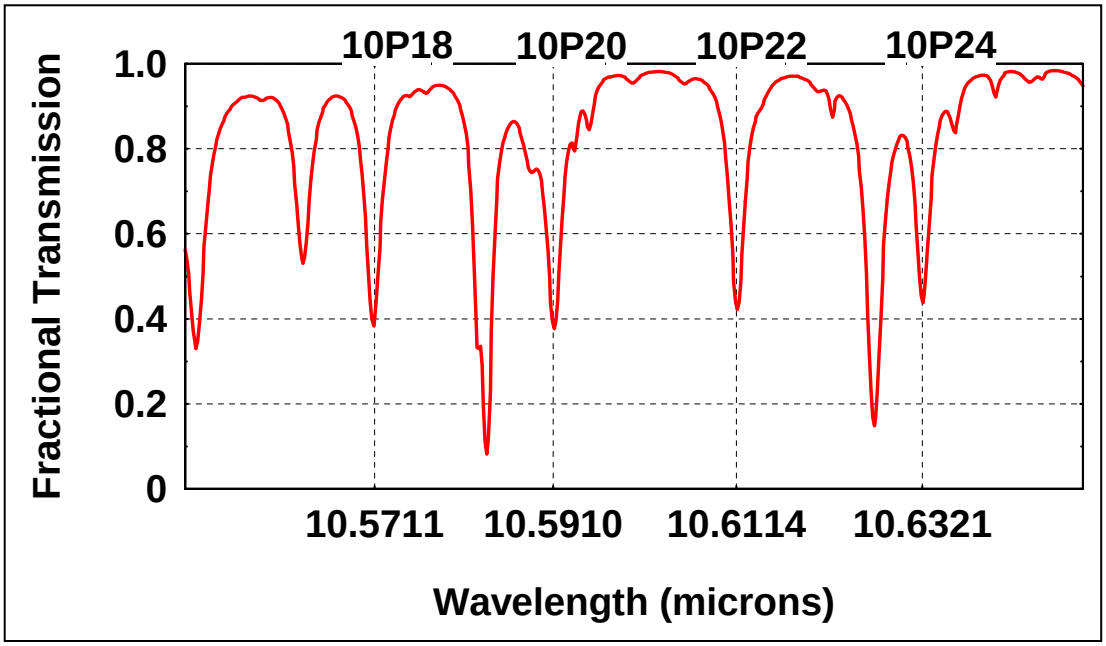

Figure 1. Atmospheric transmission of $^{12}C^{16}O_2$ laser wavelengths [6].

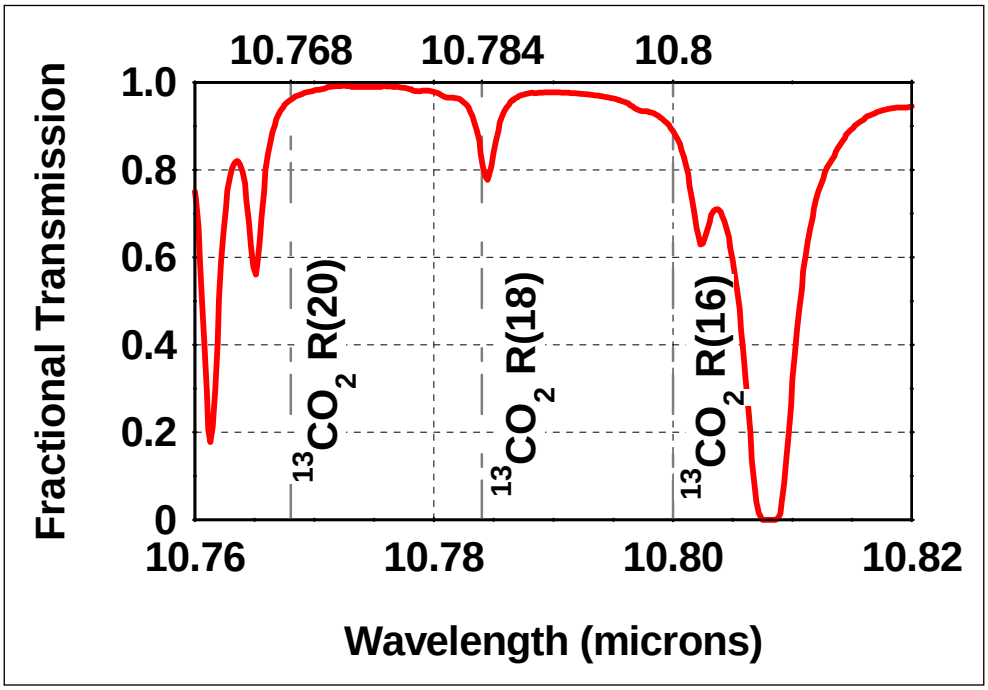

Figure 2. Atmospheric transmission of $^{13}C^{16}O_2$-isotope wavelengths [6].

1-2-2 Smoke Extinction Model

The smoke extinction model is built around the bonding theory that small particles (spherules) group together to from large particles (clusters) [6]. In this model, the term fractal dimension is used to describe how well packed spherules are within the cluster. Therefore, a fractal dimension of 1 refers to spherules just barely touching and a fractal dimension of 3 refers to a cluster with no voids. Smoke has a fractal dimension of 1.78 [6]. To calculate the transmission of radiation in smoke:

$$T = e^{-\sigma\rho L} \qquad (1)$$

where σ is the extinction cross-section, ρ is the density, and L is the total path length [6].

$$\sigma_a = 4\pi N k a^3 \,\mathrm{Im}[(M^2 - 1)/(M^2 + 2)] \qquad (2)$$

$$N = (R/a)^D \qquad (3)$$

Equation 2 is the absorption cross-section calculated for vector waves [6]. However, σ_a can be taken as an estimate for σ because the absorption cross-section is much larger than the scattering cross-section in smoke [6]. In Equation 2, k = 2π/λ and M is the complex index of refraction at wavelength λ. Equation 3 is the average number of individual spherules in each cluster [6], where R is the average cluster radius, a is the average spherule radius, and D is the fractal dimension. Figure 3 shows the transmission of three popular laser wavelengths used for communications versus smoke density [6]. For all calculations, R = 0.1-μm and L = 1000-m. Figure 3 shows that 10-μm exhibits better transmission than the other selected wavelengths.

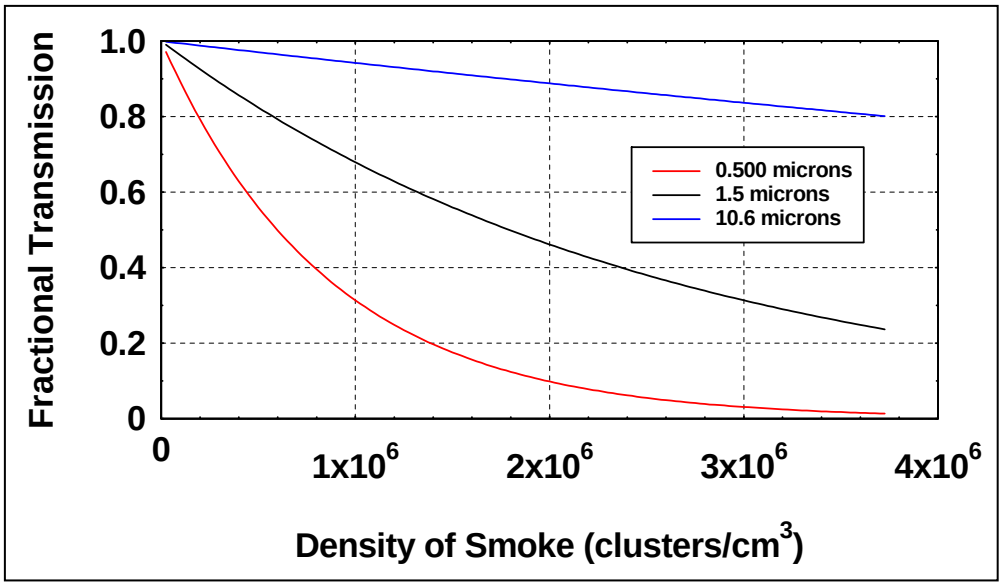

Figure 3. Transmission of commonly used laser wavelengths through smoke [6].

1-2-3 Fog Extinction Model

Finally, the extinction transmission of laser radiation in fog (water droplets), is presented in Figure 4 [6]. Here, 10-μm and 1.5-μm wavelengths are compared. Again, 10-μm is far superior. Thus, it is concluded that the 10-μm wavelength is the best wavelength to use for all-weather communication. Based on the findings in section 1-2, the R(20) line associated with the $^{13}C^{16}O_2$-isotope laser is the preference for all-weather communication.

1-3 The Thesis

Hutchinson et al. has designed and constructed a compact CW RF-driven waveguide CO_2 laser and a dielectric-waveguide Stark-effect modulator [6], [7]. The CO_2 laser is driven by a 60 MHz RF amplifier at a power level of approximately 30 watts. The modulator is based on the Stark shift of deuterated ammonia (NH_2D). Stark-effect modulation occurs when an electric field is applied to a gas molecule that has a substantial polarization. In this case, an applied electric field changes the energy spacing of the molecular levels, thereby changing the optical frequency or wavelength that is absorbed by the gas [6].

Hutchinson et al. successfully characterized a borosilicate glass waveguide Stark-effect modulator that measured 20-cm in length with an inner diameter of 0.9-mm [6], [7]. This thesis used a borosilicate glass waveguide Stark-effect modulator that is 36-cm in length and has an inner diameter of 1.8-mm. The increased size of the waveguide allowed for greater modulation amplitude. The longer waveguide Stark-effect modulator was successfully characterized, and for the first time an RF signal has been transmitted. Thus, a working prototype Stark-effect modulator has been developed.

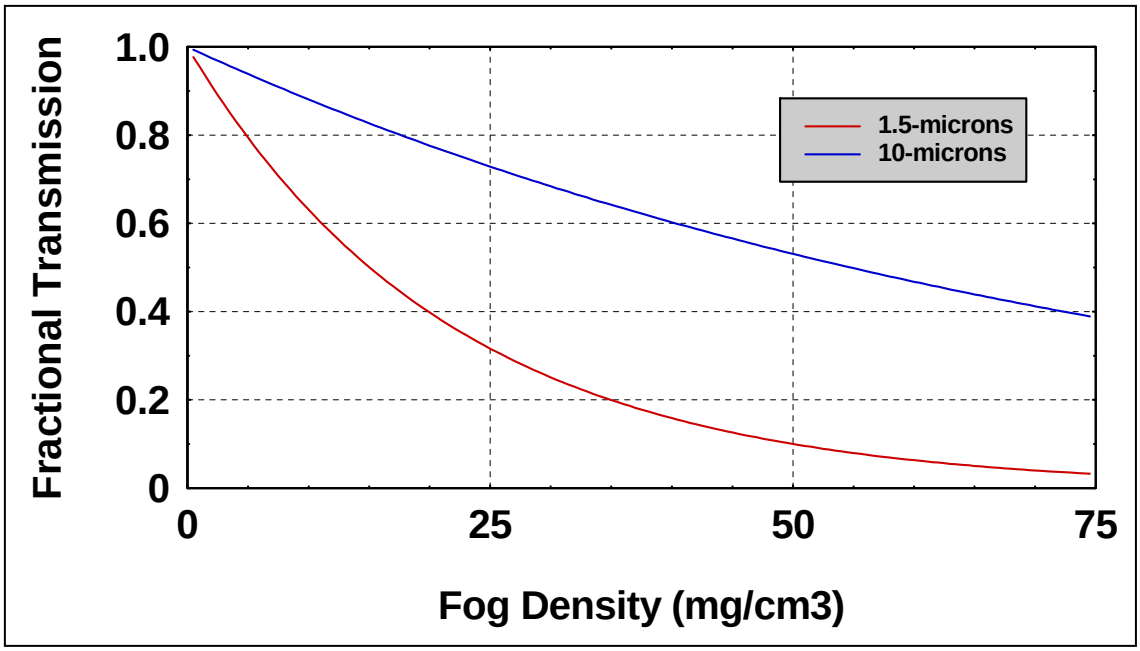

Figure 4. Transmission of commonly used laser wavelengths through fog [6].

A Stark-effect modulator is better for LWIR communications than other modulators. Electro-optic crystal modulators require a very large voltage (>1000 to 5000 volts). This voltage requirement makes high frequency modulation very difficult to achieve [6]. Acousto-optic Bragg cells are another modulation option. They are limited to modulation frequencies less than a few MHz [6]. A Stark-effect modulator requires less voltage for operation. Thus, it can operate at much higher frequencies. Also, the cost of an electro-optic crystal or an acousto-optic Bragg cell is in the thousands of dollars. A Stark-effect modulator may be produced for a few hundred dollars. The facts presented in chapter 1 are the motivation for undertaking this project.

Chapter 2:

Literature Review

The focus of this thesis is the development of a working prototype Stark-effect modulator with an application for communications. Therefore, the literature reviewed mainly identifies previous attempts to use the Stark-effect for modulation. Much of this research originated in the mid 1940's. At that time the Stark-effect was used for the technique of microwave spectroscopy and was very limited in the infrared region. This was due to poor resolution of the conventional spectrometers compared to the magnitude of the Stark shifts [14]. By the late 1960's and through the 1970's many authors were able to study Stark spectroscopy in the infrared region with the development of infrared lasers. Many of these studies led to the foundation for creating a Stark modulator to incorporate into a communication system.

Before focusing on previous studies, modulation, as it applies to communication needs to be understood. In general, modulation causes a spectral shift in a signal and is used to gain advantage in communications [11]. Two examples of this are discussed as follows.

1. If several signals, with the same frequency band, are transmitted simultaneously over the same transmission medium, they will all interfere. Consequently it will be impossible to separate or retrieve them at a receiver. Therefore, a modulated signal can be transmitted to shift the signal spectrum; giving each signal its own unique carrier frequency. Once the modulated signal reaches the receiver the signal is demodulated.

This is how radio stations transmit their signals and is known as frequency-division multiplexing [11].

2. The antenna size must be of the order of the wavelength of the signal to be radiated. Since audio signals have low frequencies and large wavelengths, impracticably large antennas would be required. Modulating the signal to a higher frequency and smaller wavelength helps solve the problem [11].

The remainder of this chapter will focus on the development of the Stark effect from a spectroscopic tool to being used for optical communication.

2-1 Microwave Spectroscopy

Townes and Schawlow are two of the earliest pioneers of microwave spectroscopy [15]. Much of their literature takes a theoretical approach as to how a molecule is affected by the Stark-effect. They define the Stark-effect as being the change in the spectrum of a system, which may be observed when the system is subjected to an electric field. Therefore, the effect an electric field has on the rotational energy levels of a molecule can be described in classical terms, but require a quantum-mechanical approach for a detailed understanding [15]. Using a quantum-mechanical approach, the shift in energy of a given level for a nonplanar symmetric top molecule is given by Equation 4 [15].

$$\Delta W_1 = -\mu_1 E \frac{MK}{J(J+1)} \qquad (4)$$

The shift in energy given in Equation 4 depends on the molecular dipole moment μ_1, the electric field strength E, and the quantum numbers J, M, and K. This energy shift which is proportional to the electric field strength is the linear or first-order Stark-effect. The

second-order effect takes into account the small changes in the molecular wave function due to the field. However, unless K = 0 the second-order energy will be so small compared to the first-order that it will be unimportant. When K = 0, the second-order energy for a symmetric molecule is simplified to Equation 5 [15].

$$\Delta W_2 = \frac{\mu^2 E^2}{2hBJ(J+1)} \frac{J(J+1) - 3M^2}{(2J-1)(2J+3)} \qquad (5)$$

Besides Townes et al. [15], Karplus [9] also observed frequency modulation in microwave spectroscopy. This work would later be expanded on by P.C. Claspy et al. [3] as the Stark-effect applies to vibrational-rotational spectra [3]. Karplus developed a theoretical description of the absorption coefficient of a gas as it relates to the density matrix of that gas. This description is described through Equation 6 [9].

$$\alpha(t) = 4\pi(\omega / \hbar c) \sum_{g,\lambda} \left| Pmn^{g\lambda} \right|^2 (\rho_{n\lambda}{}^0 - \rho_{mk}{}^0) \times \operatorname{Im} f(\omega_{mn}{}^{g\lambda}, \omega; t) \qquad (6)$$

The *Pmn* in equation 6 refers to the component of the dipole moment where g and λ are degeneracy indices. The function $f(\varpi_{mn}{}^{g\lambda}, \varpi; t)$, determines the shape of the absorption line in equation 6. Finally, the density matrix is represented by $(\rho_{n\lambda}{}^0 - \rho_{mk}{}^0)$. The density matrix involved with the absorption coefficient is obtained from its equation of motion, which takes into account a possible time-dependence of the resonant frequency of the molecule and of the frequency of the exciting radiation. Karplus goes on to take the shape of the absorption line for slow, weak, sinusoidal, and square wave modulations. This is done by evaluating the function that determines the shape of the absorption line.

Applying slow modulation, Karplus states that the line has the same shape as if there was no modulation present [9]. The only observable difference is that the

absorption peak is shifted. During weak modulation, a low modulation frequency represents an effective differentiation of the absorption line shape obtained with slow modulation [9]. Using sinusoidal modulation Karplus predicts a series of absorption lines separated by some frequency [9]. Finally, in square wave modulation, the simultaneous observation of two absorption lines, corresponding to the two values of the resonance frequency in the two half-cycles is predicted [9].

Section 2-2 will take the foundation the previous authors set and use them for observations in the infrared region.

2-2 Infrared Spectroscopy

Brewer et al. presented a spectroscopic technique based on the Lamb dip [2]. This investigation into the infrared Stark spectra of $N^{14}H_2D$ reported a rapid Stark tuning rate (frequency vs. applied field) and relatively high absorption coefficient. The research indicates the possibility of obtaining substantial modulation depth with relatively low field strength and short path length [9]. Brewer's method resulted in a unique vibration-rotation line assignment and its transition matrix element. Finally, a method to probe ground-and excited-state Stark splitting with precision was observed [2].

Their experiment examined the vibration-rotation spectrum of the $N^{14}H_2D$ molecule in the ν_2 vibration using the *P*(20) line of a CO_2 laser at a frequency of 944.191-cm^{-1} [2]. The transition was identified as $4_{04}(\alpha) \rightarrow 5_{14}(s)$ in the asymmetric rotor notation [2]. Initially, the CO_2 laser was free running and was not stabilized in any way. The laser operated CW on a single longitudinal mode with 75-MHz, with linear polarization, and with an output power of a few W/cm^2 or less. However, for low-noise

Lamb signals an exceptionally stable free-running CW laser was required. The laser beam passed through a cell containing $N^{14}H_2D$ and Stark plates made of glass and vacuum-coated with aluminum on the inner surface. The narrowest lines were observed with plates 12.5-cm long by 2.5-cm wide and separated by polished ($\lambda/10$) quartz spacers 0.1519-cm thick. These plates were oriented so that the Stark field was either parallel or perpendicular to the optical field direction corresponding to the selection rules $\Delta M=0$ or $\Delta M=\pm 1$ [2]. This experiment produced Stark splitting as narrow as 1.5-MHz (within a Doppler width of 82-MHz) [2]. This was the first time this was observed in an optically excited state using the Lamb dip.

Shimizu [14] also performed an infrared spectroscopy experiment. He reported on Stark spectroscopy of the $^{14}NH_3$ ν_2 band by 10-μ CO_2 and N_2O lasers. The advantage of using these lasers to study vibrational spectrum is that they have an oscillating line in every 1 or 2 wavenumbers covering most of the 9- and 10-μ region [15].

Shimizu's experiment used a 2-m flowing gas laser system with a cavity length of 2.6-m. One of the mirrors was replaced with a grating in order to select the transition by changing the angle of the grating. With this arrangement in place it was possible to obtain oscillations between the *P*50 and *R*50 lines of the ν_3-ν_1 band of the CO_2 laser [15]. Also, lines from *P*42 to *P*5 and from *R*5 to *R*39 of the ν_3-ν_1 band of the N_2O laser were achieved [14]. From this point, the laser beam was passed through a cell measuring 40-cm long and maintained at a pressure of ~10^{-2}-10^{-3}-torr. The cell had parallel aluminum electrodes with an electric field of 45-V/mm. The modulation voltage was kept around 40-V peak to peak at a frequency of 5-kHz for most lines, while the voltage was

increased for a few of the weaker lines. Finally, a Ge:Au photoconductive detector was used to monitor the modulated signal. This experimental arrangement provided about 100 coincidences between NH_3 lines and laser lines [14]. Also, the NH_3 line positions relative to the laser lines are calculated using the data for the dipole moment obtained by the experiment [14].

2-3 Stark-Effect Modulation

Using the basis that previous researchers developed, Landman and Marantz began experimentally determining which electro-optic gases would modulate a laser beam [10]. They began this evolution of Stark modulation for two reasons. The advantage of gases for modulation lies in the narrow lines that can be obtained, and the simplicity to construct and incorporate a Stark cell into a system [10]. First, they said that four criteria must be met to achieve a high modulation index in molecules for modulation [10]. (1) Molecules must have a large dipole moment. (2) Molecules that are asymmetric top-molecules with slight asymmetry are good candidates if the Stark effect is linear at the applied field. (3) The linear Stark effect should be either in the lower state, upper state, or both. (4) The laser line and the absorbing line should be in coincidence to within one or two Doppler widths of the absorbing gas.

The Stark shifts of molecular absorption can amplitude modulate, frequency modulate, line switch, and cause polarity changes to the laser output. However, Landman and Marantz only investigated amplitude modulation because of its application to optical communications using a CO_2 laser [10]. Their experimental set up involved a 1-m sealed-off CO_2 laser with external mirrors, one of which is a diffraction grating.

Table 1. Experimental results for percentage modulation [10].

Gas	Vibration	Dipole Moment (D)	CO2 Wavelength (μ)	Modulation (%)	Pressure (Torr)	Field (kV/cm)
NH_3	[a]Symm. Deform.	1.47	10.286	0.5	6	2
CH_3BR	[b]Rock	1.80	10.612	4	3	1
CH_3F	[a]C-F Stretch	1.79	9.658	10	2	0.9
CH_3CL	[b]Rock	1.87	9.606	20	6	1.5
CH_3I	[b]Rock	1.65	10.532	4	10	2.5
NF_3	[b]Deg. Stretch	0.234	9.586	0.3	10	2.5

[a]Parallel band.
[b]Perpendicular band.

Then the laser beam was passed through a 1-m Stark cell whose plate separation was 1/8-in with a capacitance of 70-pF and an electric field of at least 1-kV/cm. A gold-doped germanium detector was used to observe the effects.

Using the experiment described above, the most promising combination of CO_2 line and Stark cell gas was the $P(26)$ 00^o1-02^o0 line of CO_2 and a line of methyl chloride [10]. More importantly, molecular Stark effects were seen in six other gases. Therefore, this led them to believe that many more gases held promise for modulation. Table 1 shows their findings. In order to increase the modulation depths presented in Table 1, improvements to the modulator are required. It would have to be much shorter and narrower to reduce the capacitance and thus the power requirement, which equals V^2Cw (V=applied voltage, C=total capacitance, w= bandwidth) for an impedance match [10].

P.C. Claspy et al. performed both a theoretical and experimental study of the time-dependent molecular Stark effect and its application to the modulation of CO_2 laser radiation [3]. First, their theoretical approach took ideas that Karplus [9] developed for

microwave spectroscopy and altered it to be applicable to absorption of laser radiation in the infrared. They used a density matrix approach to develop a quantum mechanical description of the effect of a time-varying electric field on the absorption coefficient and refractive index of a molecular gas near an absorption line [3]. Equation 7 describes a single Lorentzian line with a time-varying center frequency moving synchronously with the Stark field [3].

$$\alpha(\varpi, t) = \frac{\omega |p_{mn}|^2}{c\varepsilon_0 \hbar} \frac{(1/\tau)}{[\omega_{mn}(t) - \omega]^2 + \gamma_s^{\ 2}} \tag{7}$$

where

$$\omega_{mn}(t) = \frac{W_m(t) - W_n(t)}{\hbar}$$

ω	frequency of light,
p_{mn}	absorption transition moment,
$1/\tau$	small-signal absorption linewidth,
$\omega_{mn}(t)$	transition frequency,
γ_s	homogeneous linewidth,
$W_i(t)$	molecular energy levels in time.

After their theoretical investigation Claspy determined the basic characteristics of the time-dependent molecular Stark effect in a CO_2 laser modulation application [3]. They used an 80-cm long laser that consisted of a 4-m gold surface mirror and a 1800 lines-per-inch diffraction grating blazed for 10-μ. Also, they used a piezoelectric driver to scan lines. Next, the modulator measured 30-cm long and 3.8-cm wide with a plate separation of 1 cm and windows made of NaCl. The plates were in a parallel configuration and were made of aluminum. The modulator gas used was methyl chloride for $P(26)$ of the (00^o1) - (02^o0) CO_2 band. The experimental results obtained show non-

dispersive modulation at frequencies up to 30-MHz [3]. They also found that the response of modulation depth to Stark field amplitude is separated into linear and nonlinear regions [3]. Finally, this work concluded that this method could effectively be used in the modulation of CO_2 laser radiation because modulation depths of greater than 80% were observed.

Johnston and Melville reported that deuterated ammonia NH_2D can be used to modulate the strong 10-μ *P*(20) line of a CO_2 laser [8]. This is the same approach this thesis has taken. Therefore, the theoretical model based on Stark-effect theory, used to characterize the Stark modulator in this thesis originated from Johnston and Melville [9]. This model is presented in the appendix.

While the laser line and the gas are the same as this thesis, the experimental arrangement is somewhat different. Johnston and Melville used a CO_2 laser that was 1-m in length and tuned to the 10.6-μ *P*(20) line by means of a grating. Their beam passed through a Stark cell that was made of a glass cylinder containing polished aluminum plates 19.7-cm long, 2.5-cm wide, and separated by 0.109 ± 0.003-cm by means of glass spacers. The aluminum plates were rounded to avoid breakdown of the deuterated ammonia and NaCl windows were attached to the Stark cell. To create a Stark field in the cell a small sinusoidal probe field of constant amplitude at 400-Hz was applied to the cell as a larger dc bias field swept the absorption line across the laser frequency. Once the laser beam passed through the cell it was detected with an SBN pyroelectric detector. Also, similar to this thesis, NH_2D was created by mixing NH_3 and ND_3 in a Stark cell. The exchange of hydrogen and deuterium occurs quickly; and reaches equilibrium in less than one minute.

The data provided from this experiment gave values for the absorption coefficient at line center (γ_M) and the pressure-broadening coefficient (C) which both apply to the M=4 Stark component. The absorption coefficient at line center was determined by measuring the absorption at line center as a function of pressure in several mixtures of ND_3 and NH_3. The absorption at line center was found to be γ_M=0.033 cm^{-1} [8]. The observed pressure-broadening coefficient was found by measuring the line width as a function of pressure [8]. Its value was found to be C=32.5-MHz*$Torr^{-1}$ [8]. With these values at hand the maximum intensity modulation to be expected for a 19.7-cm cell with 20-V rms applied signal can be calculated using Equation 8 [8].

$$I = I_0 e^{-\gamma l} \tag{8}$$

where

$\gamma = \gamma_M CPb/(\varepsilon^2 + b^2)$=absorption coefficient,
l= length of cell,
P= pressure,
b= linewidth,
ε= frequency offset of line center from the laser frequency.

The result is $\Delta I/I_0$=48%. The experiment produced a modulation depth of 40%; therefore, these values are in good agreement with one another.

C.K. Asawa and T.K. Plant [1] took a slightly different approach than Johnston and Melville [9]. After studying low-pressure Stark resonance spectra of $N^{14}H_3$ with 25 of the more intense P and R lines in the 10- to 11-μm range they observed intense Stark resonance absorptions of the R(18) and R(24) lines and a weaker absorption of the R(26) line of the $C^{13}O_2^{16}$ laser by $N^{14}H_3$ in a Stark cell [1]. Measurements were taken of the absorption versus applied voltage to the Stark cell for all three lines

mentioned previously. The *R*(18) line had absorption peaks occur at 1000, 1200, and 1500 Volts of applied voltage to the Stark cell, which corresponded to the $\Delta M=0$ transitions between $|M|=6,5$, and 4 levels. The *R*(24) line had its lowest Stark field resonance appear at 1800 Volts of applied voltage for $|M|=2$. Finally, the *R*(26) line occurring at 2400-V was not identified. In the process they also performed a wideband modulation experiment with an $N^{14}H_3$ Stark cell and the *R*(18) line. There were many promising results from this experiment. First, the Stark cell measured only 10-cm long and only a modest amount of power (<1 W) was required to attain useful modulation depth at high data rates [1]. Finally, and most important, their Stark modulator reproduced 180-Mbit/s random words [1]. They felt that the modulator could attain even higher bit rates with useful modulation depths.

T.K. Plant continued his investigation, but this time with R.L. Abrams [13]. They reported new values for the magnitudes of the pressure broadening and linear absorption coefficients. This was done for the Stark tunable $(0_a, 4_{04}, 4) \rightarrow (1_a, 5_{05}, 5)$ transition in $N^{14}H_2D$ using a CO_2 laser operating on the *P*(20) 10.59-μm line [13]. Plant and Abrams used this modulating gas because of its unique energy structure that is useful for laser modulation, laser stabilization, and nonlinear optical interactions that resulted in a single sideband modulator operating at microwave frequencies [13].

Their modulator grounded one plate while driving the other with a 9-Hz 300-V peak-to-peak square wave that was imposed on a slow sawtooth sweep varying from 240- to 350-V. They measured absorption line shapes, and extracted linewidths, for Stark cell pressures varying between 50-mTorr and 10-Torr. They also created $N^{14}H_2D$ gas by mixing two parts $N^{14}H_3$ and one part $N^{14}D_3$.

Two methods were used to derive the pressure-broadening coefficient. First, the homogeneous linewidths for various pressures generated a best straight-line fit through zero to these values [13]. The slope of this line resulted in a pressure-broadening coefficient of 40.2 $\pm$ 0.4-Mhz/Torr [13]. The other method to determine the pressure-broadening coefficient examined the pressure dependence of the line-center absorption coefficient [13]. This resulted in a value of 40.3-Mhz/Torr [13]. Finally, from the predicted asymptotic behavior of the line-center absorption coefficient at high pressures the absorption coefficient was extracted to be 0.028-cm^{-1} [13].

2-4 Stark-Effect Modulator at ORNL

Hutchinson et al [6], [7] used a borosilicate glass waveguide Stark-effect modulator that measured 20-cm long with an inner diameter of 0.9-mm. The results, which are explained in section 2-4-2, resulted in a successful characterization of their Stark-effect modulator. To improve the modulation amplitude a longer Stark-effect waveguide made of borosilicate glass was needed. This thesis extends the preceding work performed by Hutchinson et al [6], [7] by characterizing the longer Stark-effect modulator and by applying RF modulation to the system for the first time. The foundation for Hutchinson's work was the result of the previously describe work.

2-4-1 Theory of Stark-Effect Modulation

Stark-effect modulation occurs when an electric field is applied to a gas molecule. Basically, the electric field changes the energy spacing of the molecular levels. In turn, the energy spacing changes the optical frequency and wavelength absorbed by the gas. The molecular gas chosen to interact with the CO_2 laser radiation is partially deuterated ammonia, specifically, NH_2D. This molecular gas is chosen because it has a

molecular absorption resonance near the 10.59 micron line of the CO_2 laser

Figure 5 shows the theoretical transmission of a 30-cm cell containing 2-Torr of NH_2D [6]. The blue line represents the transmission of $NH_2D$when no electric field is applied. The red line depicts the transmission of NH_2D when an electric field of 350-V/mm is applied to the pressurized cell. Finally, the *P*(20) 10.59-μm CO_2 laser line is located at zero difference frequency. Notice how the absorption line is split into nine Stark components. They will be classified as M = 0, ±1, ±2, ±3, ±4, with the M=0 component roughly in the center at a frequency difference of 2189 MHz and the M= ±4 components on the outer edges. If the electric field is increased the transmission curve will change, as shown in Figure 6. With the electric field being increased to 380 V/mm, in Figure 6, the absorption line near M=-4 comes into coincidence with the 10.59 micron laser line. From Figures 5 and 6, digital modulation is predicted to be achievable by setting a steady field at 365 V/mm and applying a 30-V digital signal to switch the transmission of the cell between 75% and 90% states. Also, if the length of the cell is increased then the modulation amplitude may exceed 30% [7].

2-4-2 Experimental Results

Hutchinson et al. characterized a dielectric Stark-effect modulator [7]. The waveguide material was borosilicate glass and measured 20-cm with an inner diameter of 0.9-mm. The modulator was filled with 8-Torr of NH_2D, and the transmission (measured signal) as a function of the applied voltage was measured. An AC bias waveform was generated by applying a square wave drive voltage from a signal generator to an iron-core step-up transformer. The transformer was a 110 VAC to 6.3 VAC filament transformer operated in reverse.

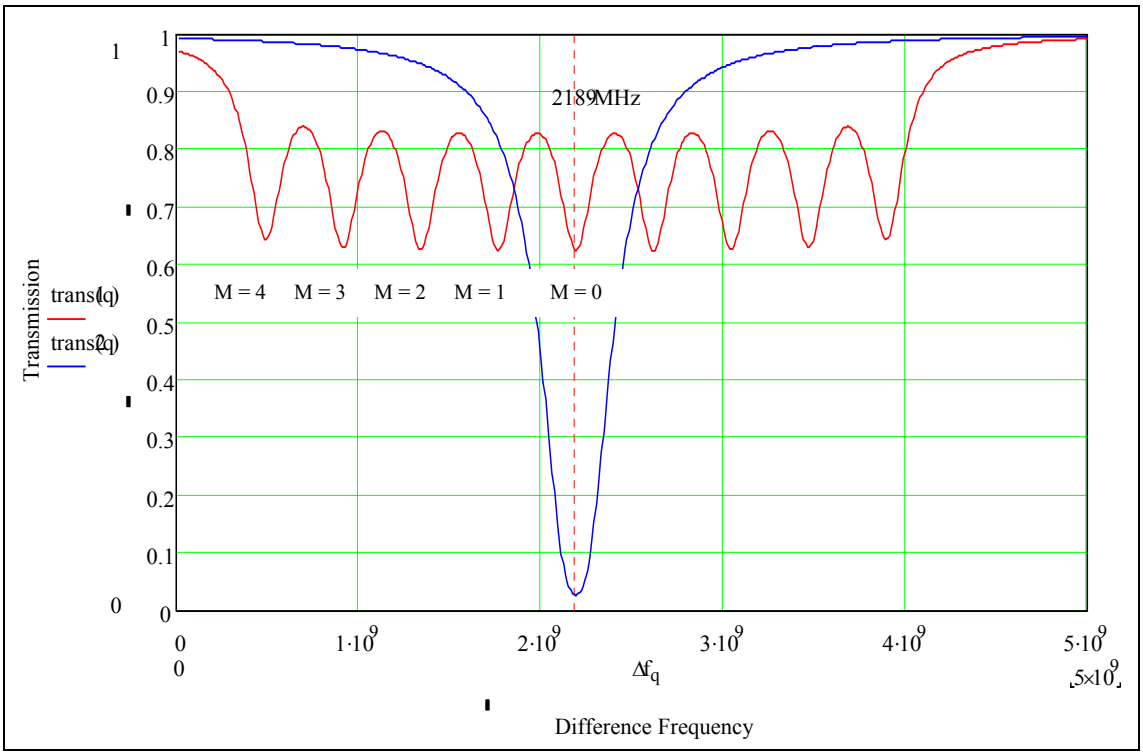

Figure 5. The simulated transmission of NH_2D in a 30-cm cell at 2-Torr. The blue curve represents the transmission with no electric field applied. The red curve shows the simulated transmission when an electric field of 350 V/mm is applied to the cell [6].

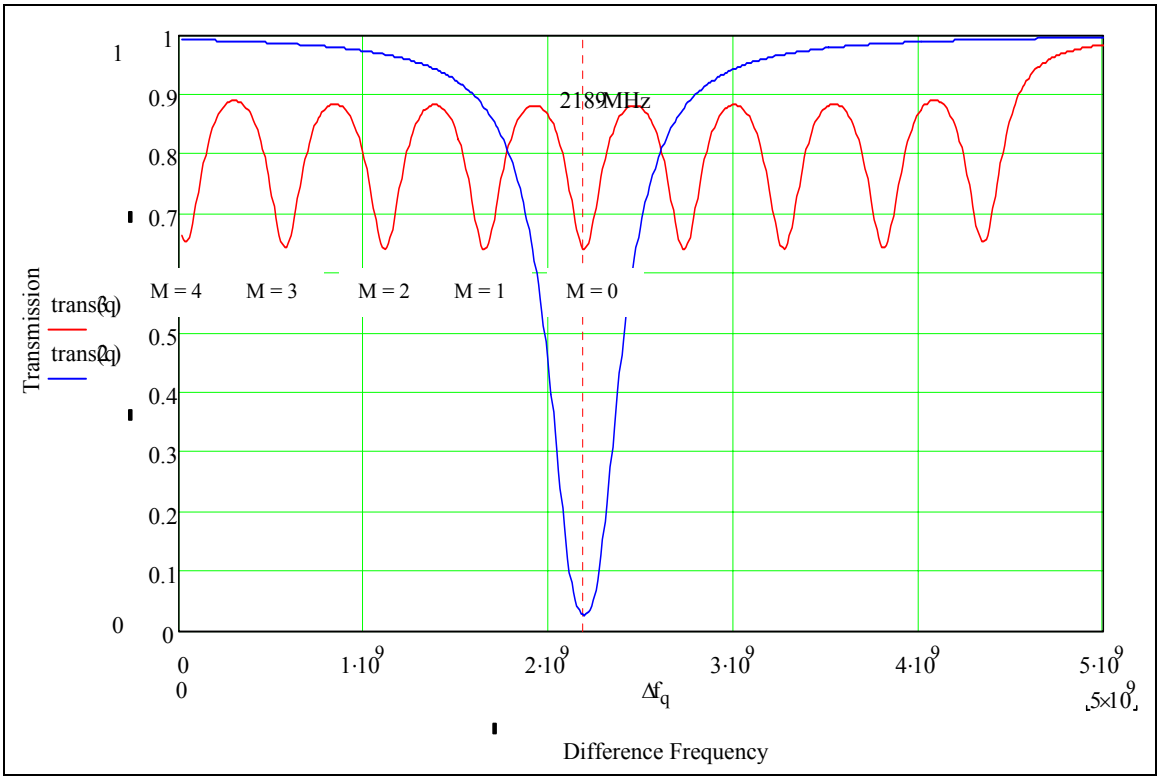

Figure 6. The simulated transmission of NH_2D in a 30-cm cell at 2-Torr with a larger applied electric field than Figure 5. The blue curve represents the transmission of NH_2D when no electric field is applied. The red curve shows the transmission of NH_2D when an electric field of 380 V/mm is applied to the cell [6].

Figure 7 compares Hutchinson's [7] experimental results to the theoretical transmission curve. Also, a peak modulation index at approximately 30% resulted. The results are in excellent agreement with the theoretical model provided by Johnston et al. [8]. A MathCad representation of the model is found in the appendix. This model takes into account the cell length, e-field enhancement, and the deuterated ammonia fraction.

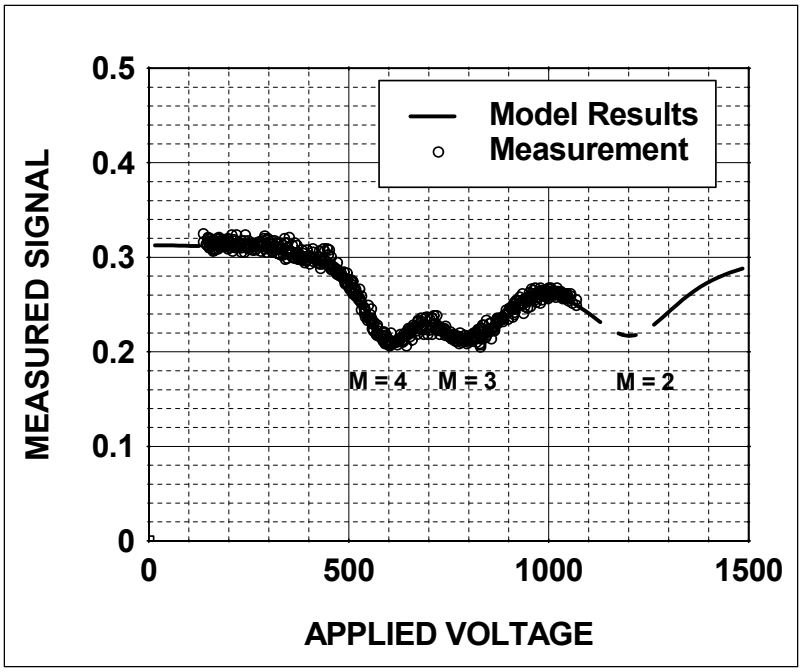

Figure 7. The transmission (measured) signal versus applied voltage in a 20-cm long cell filled with 8-torr of NH_2D. This result is provided from reference [7]. The theoretical model and recorded data is in excellent agreement with one another.

Chapter 3:

Research

This project was accomplished by using a compact CW RF-driven CO_2 laser and a dielectric-waveguide Stark-effect modulator. A description of the CO_2 laser, Stark-effect modulator, and overall experimental arrangement will be outlined. This experimental arrangement was used to transmit an RF signal, for the first time.

3-1 CO_2 Laser

The laser shown in Figure 8 is a compact cw RF-driven, air-cooled, sealed-off waveguide CO_2 laser. This design is similar to a laser developed by Walsh [16]. Beginning from the right-hand-side of Figure 8 and moving left the laser cavity will be explained. First, the cavity consists of a 0.5-inch diameter 3-meter radius-of-curvature concave ZnSe 95% reflective output coupler. This coupler is attached to the ceramic waveguide [6]. The attachment was made by sealing a brass fitting with epoxy to the waveguide. This brass fitting was soldered to a brass bellows. Finally, the other end of the brass bellows was sealed to the coupler. The ceramic waveguide has an inner diameter of 2.4-mm. The cavity length is 30.5-cm, making it very compact. The other end of the waveguide is closed off with a ZnSe Brewster window that is attached with epoxy, and ground to the Brewster's angle. Finally, the back end of the laser has a 150 mm^{-1} flat grating mounted on a piezoelectric actuator in an adjustable mirror mount to alter the wavelength. The laser was adjusted to the *P*(20) line for measurements.

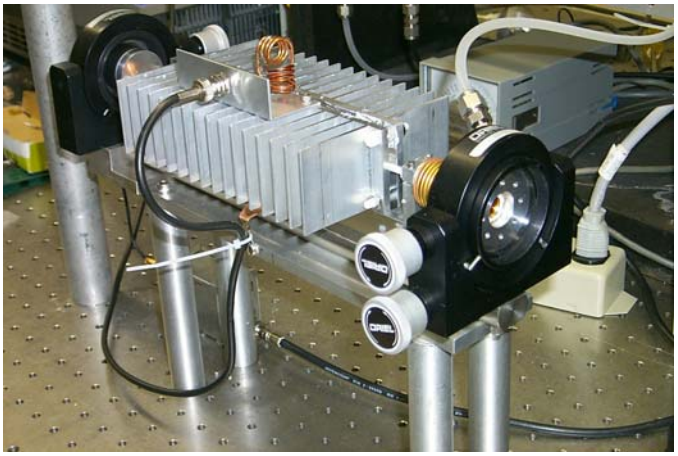

Figure 8. The RF-driven CO_2 laser used for modulation experiments [6].

The waveguide was filled with a gas mixture of $He:CO_2:N_2:Xe$, in the ratio of 77:10:10:3, respectively. Walsh also used this gas mixture [16]. During the work presented in section 2-4-2 a gas mixture of $He:CO_2:N_2:CO$ in the ratio of 65:18:15:2 was used, respectively. The ratio of this gas mixture was not thought to be optimized; therefore, $He:CO_2:N_2:Xe$ is thought to be a better mixture. This mixture was commercially purchased for a pulsed CO_2 laser. It was determined by measuring the infrared power at different pressures that the laser had its highest infrared power output (around 1 Watt) at approximately 82-torr. The laser's waveguide was filled with the aid of the apparatus seen in Figure 9. On the left side of Figure 9 is the enclosure in which the laser and other power component are housed. On the right side is the apparatus for filling the waveguide with the gas mixture. This apparatus has plumbing on the reverse side that connects the gas tank, vacuum, and laser. On the front face are knobs to fill and evacuate the system of the gas mixture. Also on the front face is a pressure meter (Wallace and Tiernan Model FA160) to conveniently view the gas mixture pressure.

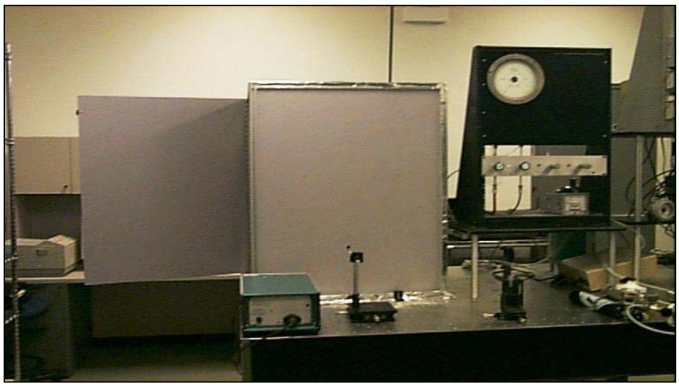

Figure 9. On the left is the laser housing. This kept the RF power from interfering with other electronics. On the right is the gas filler and evacuator.

The laser was driven at approximately 60-MHz with a power output of approximately 30-watts. From Figure 8 the two aluminum heat sinks are the most dominating feature of the laser. These not only serve as a way to cool the ceramic waveguide, but also act as RF electrodes. One of the electrodes is grounded. On the top of the laser there are two air wound inductors. One helps match the impedance of the laser to the 50-ohm coaxial cable that supplies RF power and the other acts as an autotransformer to couple RF power to the electrodes.

The system used to supply RF power to the autotransformer is shown schematically in Figure 10. Approximately 60 MHz was supplied with a signal generator (Tektronix Type 191, Serial number 005793) to an amplifier (Amplifier Research, Model 4W 1000). This amplified frequency was then sent through a wideband RF power amplifier. This RF power amplifier is a Motorola Semiconductor Product that is a 300 watt unit with a frequency range of 10 to 150 MHz [4]. The circuit board was powered by its own DC power supply (Hewlett Packard 6653A, serial number 3640A02978). To keep the wideband RF power amplifier from overheating it was mounted on a copper

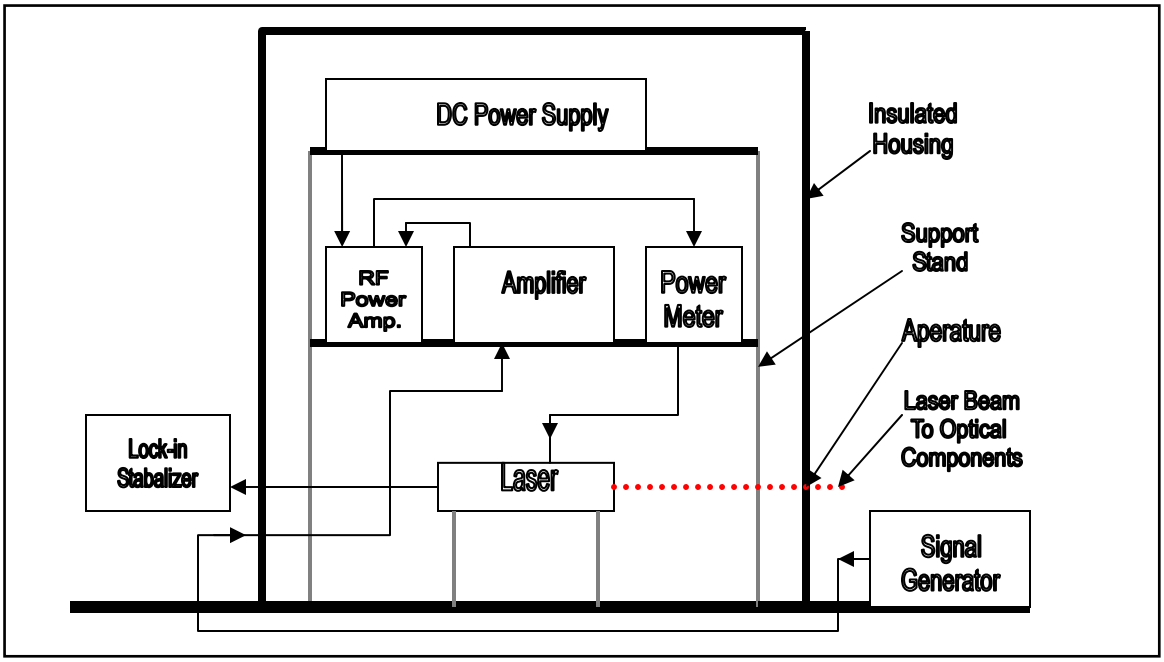

Figure 10. Schematic inside the RF insulated housing. The components that supply an RF signal to the laser are shown.

heat plate mounted to an aluminum heatsink. A cooling fan was mounted on the heatsink to cool the entire assembly. Finally, the wideband RF amplifier signal passed through a power meter (Bird Electronic Corporation) before connecting to the autotransformer and matching inductor on the laser. The back end of the laser, with the 150 mm^{-1} flat grating mounted on a piezoelectric actuator, is connected to a lock-in stabilizer (Lansing, model 80.215) with a SHV cable. As can be seen from Figure 9 and Figure 11, an enclosure was built to house the laser and most of the components mentioned above. Only the RF signal generator and lock in stabilizer are outside of the housing. The housing is made of insulated panels and wire mesh screening (for cooling) and joined together with structural rails. This was done to keep the RF signal from interfering with the modulator and other pieces of electronics. One side of the housing has a door on it for access and this side is shown in Figure 11.

3-2. Stark-Effect Modulator

As noted in chapter two, most Stark-effect modulators consist of two parallel electrodes that are placed inside a dielectric tube that is typically made of glass or ceramic and is under partial atmospheric pressure. Expansion of a laser beam through a structure with closely spaced electrodes causes a loss of light due to vignetting of the beam by the electrodes [7]. Therefore, this project design used a hollow dielectric glass tube that acts as a dielectric waveguide. The tube is held between two metallic electrodes. The laser beam is focused into the tube and the size of the focused beam is designed to match the EH_{11} low order mode of the waveguide [7]. The dielectric waveguide transmits over 90% of the incident laser radiation to minimize the loss of light. Figure 12 and 13 show schematics and Figure 14 is a picture of the modulator.

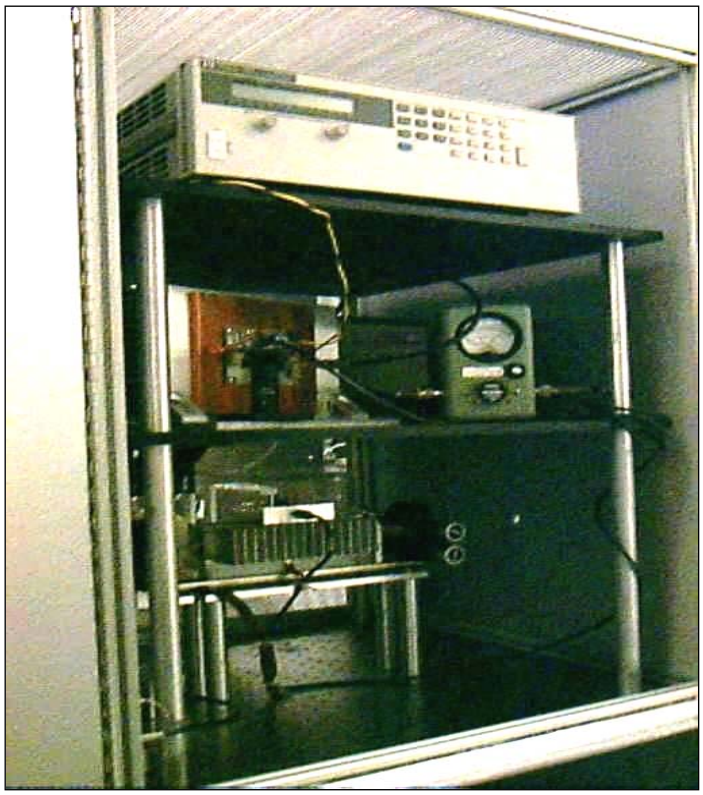

Figure 11. Inside the RF insulating housing. The laser is located at the base of the picture. Some of the components that supply power to the laser are shown.

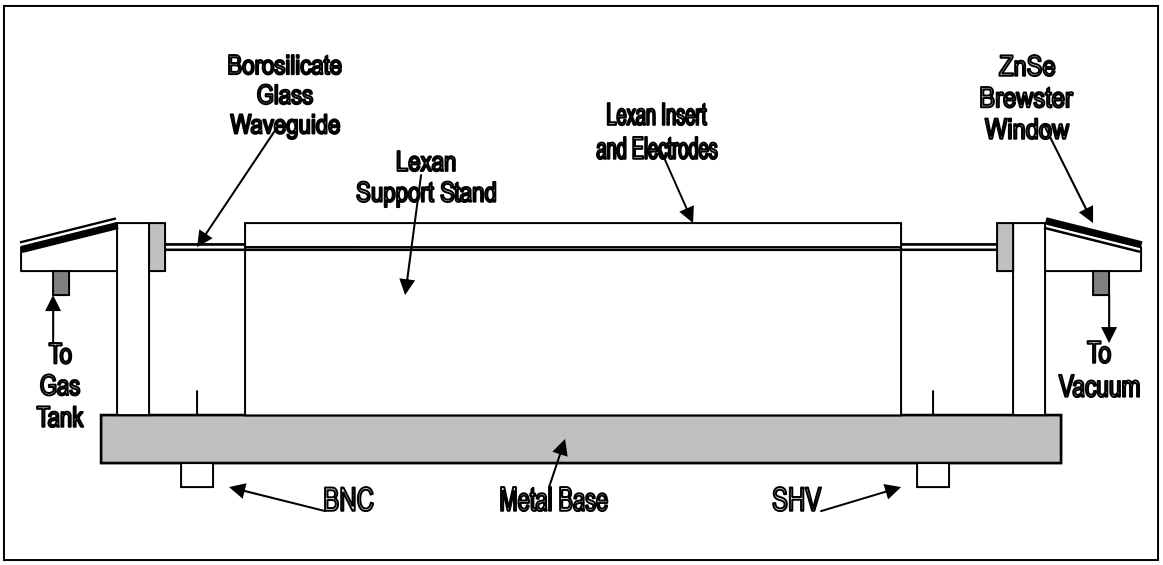

Figure 12. Side view of the Stark-effect modulator. There are two SHV connections. They are both used to apply an AC bias signal. Also, there are two BNC connections. One is used to apply an RF signal. The other is used to monitor the AC bias voltage.

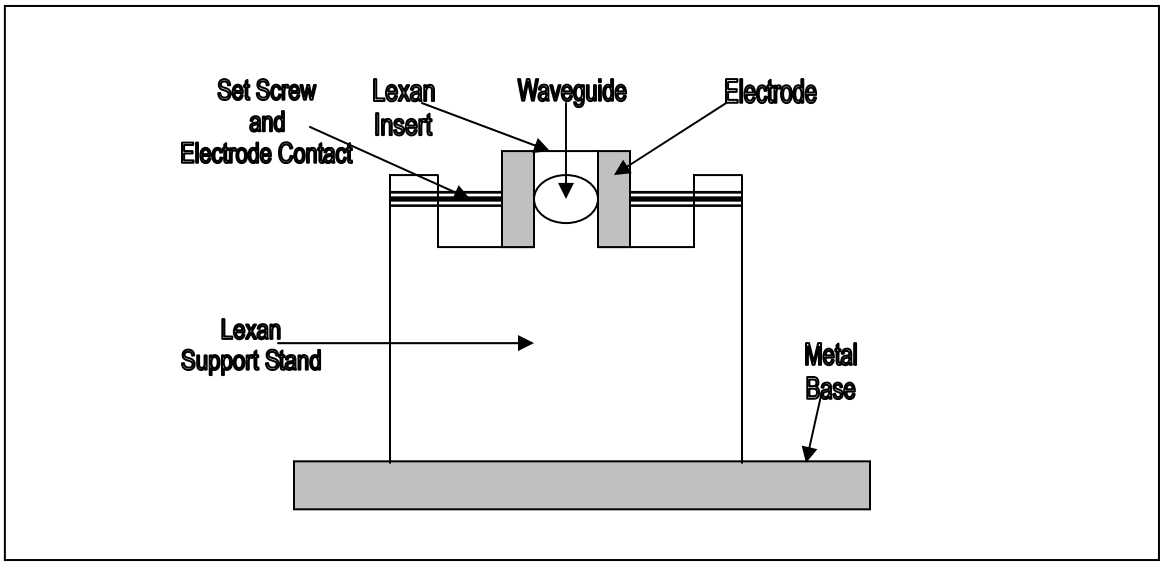

Figure 13. Cross section of the Stark-effect modulator. The AC bias voltage is supplied to the set screws. Since the set screws make contact with the electrodes, this is how the AC bias voltage is supplied to the electrodes.

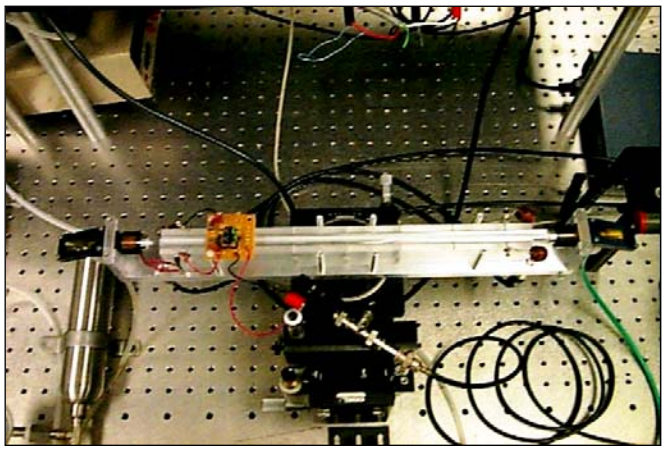

Figure 14. Picture of Stark-effect modulator.

The waveguide material used in the Stark-effect modulator is borosilicate glass. It measures 36-cm long with an inner diameter of 1.8-mm and an outer diameter of 3-mm. Both ends of the waveguide are sealed to the ZnSe windows. This seal was created by machining cylindrical aluminum connectors that fit around the ends of the waveguide and were sealed in place with epoxy. Then these ends were fastened to the ZnSe Brewster window casings with manufactured bolts designed for the casings. This was required to provide a method for filling and evacuating the cell. The ZnSe window cells were connected to the mixed gas tank and the vacuum pump as shown in Figure 12. The waveguide is suspended between two 1-cm wide by 36-cm long flat aluminum electrodes. To mount the waveguide, two pieces of lexan were used. These are labeled Lexan Support Stand and Lexan Insert in Figure 13. They not only provide support, but also align the electrodes and enhance the electric field in the waveguide. The electrodes were held in place with set screws that run the length of the electrodes. In addition, the screws near the SHV connectors were supplied with the AC bias signal. There are two

BNC connectors. One BNC plug applies the RF data signal. The other BNC plug monitors the AC bias voltage.

3-2-1 Molecular Gas Filling

It was mentioned in section 2-4-1 that deuterated ammonia, specifically NH_2D was the first gas chosen to fill the modulator with. The NH_2D was formed by combining 2 parts ND_3 with 1 part NH_3. This was accomplished with two commercially purchased bottles of ND_3 and NH_3 and one mixing tank. A specially fabricated plumbing unit mixes the molecular gas in a mixing tank, to supply the gas to the modulator, and to evacuate the modulator into the vacuum. This device is viewed in Figure 15. The metal plate with the turning valves on the front is this device. It is placed in front of the modulator. The three tanks mentioned above are seen tied down to the optical table in the left view of this picture. A schematic view of the back side of the filling device is seen in Figure 16.

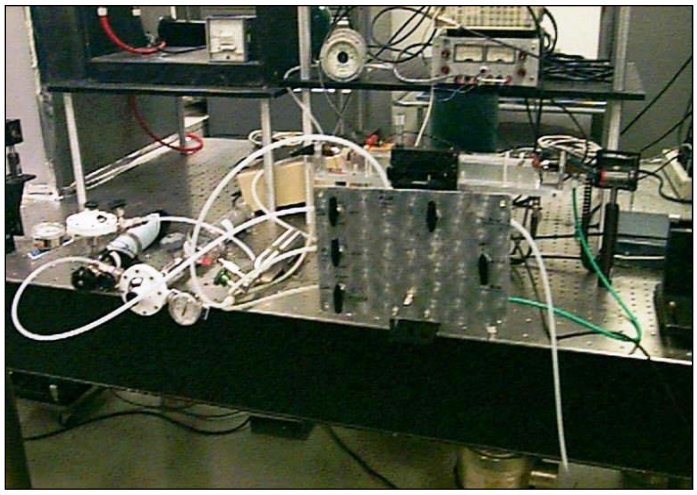

Figure 15. The NH_2D gas is formed and supplied to the modulator here.

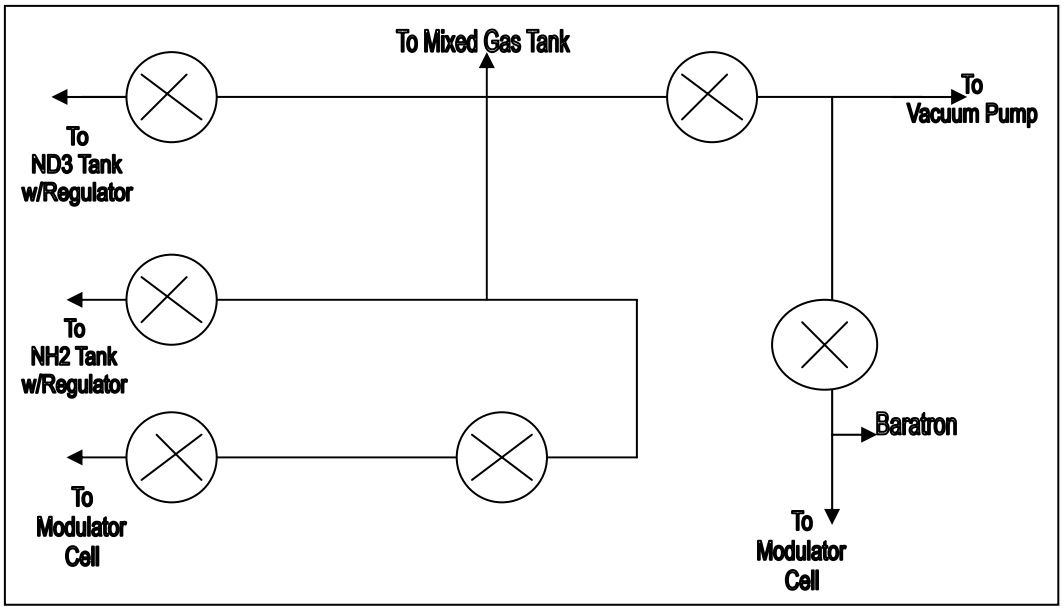

Figure 16. A schematic drawing of plumbing for the gas filling apparatus.

3-2-2 AC Biasing

A problem with the electrodes being external to the waveguide is that charge build-up results inside the waveguide from stray ions and electrons [7]. One electrode is supplied with a positive voltage while the other receives negative voltage. If a dc electric field is applied to the modulator stray electrons will be attracted to the positive electrode and the stray ions will be attracted to the most negative electrode. The resulting charge build-up in the modulator results in a cancellation of the electric field inside the waveguide. This means no modulation will occur. During the experiment performed by Hutchinson et al. [7], it was noticed that a finite time was required for the charge to build up and cancel the electric field. Therefore, an AC biasing method was developed [7]. The AC biasing was accomplished by using a circuit that generates a low frequency (around 100 to 1000 Hz) square wave.

Figure 17 is the circuit that produces the AC bias voltage. Approximately ±800-V was applied to the modulator. The amplifiers were connected to the modulator plates in a bridge configuration, meaning that each amplifier was supplied with 400-V and -400-V. The amplifiers used for this were high voltage power operational amplifiers made by APEX Microtechnology, Model PA94. The waveform produced is seen in Figure 18. In Figure 18 the applied AC bias voltage produces an AC bias signal that is only proportional to the magnitude. This is shown on the right of Figure 18. To understand this phenomenon, the selection rule for absorption says that the electric field be applied perpendicular to the electric field of the optical beam [7]. Referring to Figure 5 and 6 the polarity of the electric field is not important. For example, if the electric field is applied with the positive electrode on the right and the negative electrode on the left or vice versa, the absorption curves in Figure 5 and 6 will not be changed [7].

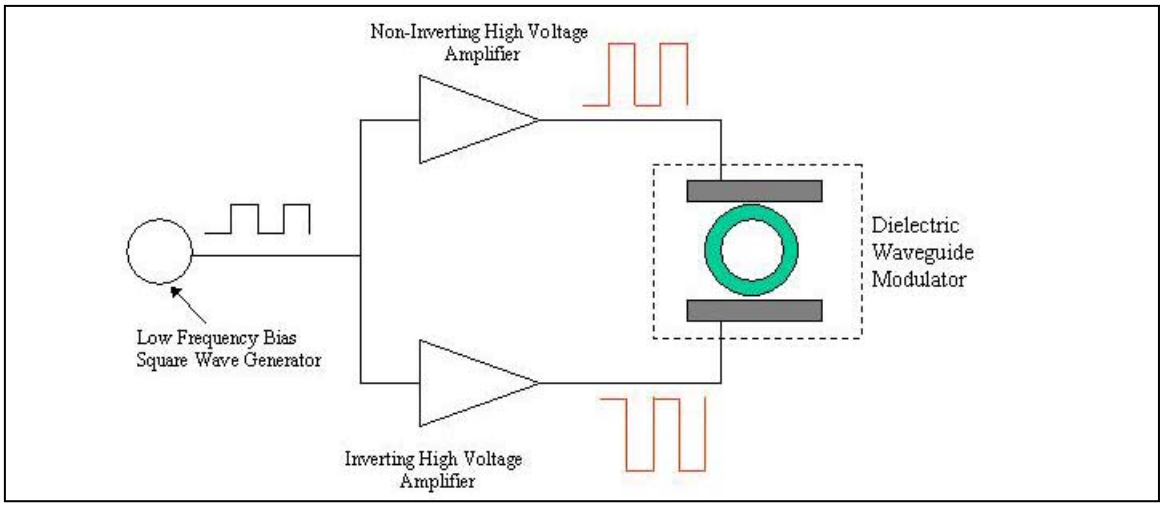

Figure 17. The bridge circuit designed for an AC bias signal. The EK19 kit made by APEX Microtechnology was used for the bridge circuit.

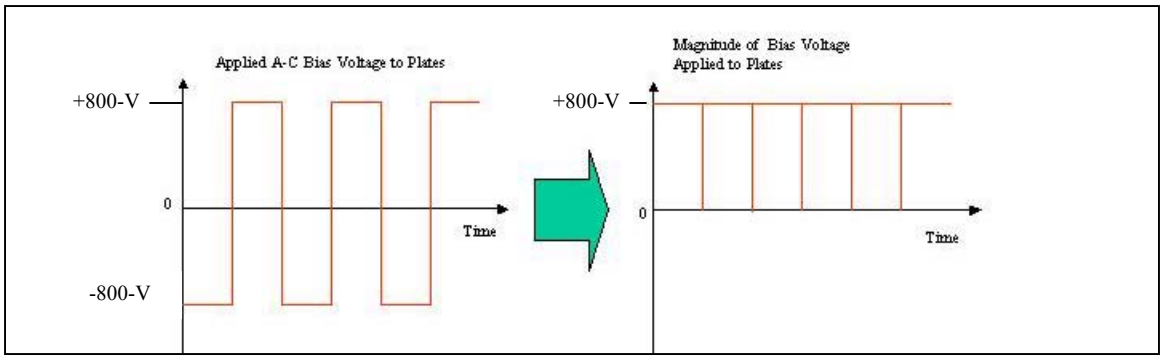

Figure 18. The applied AC bias on the left produces the equivalent to a steady "DC" bias as shown on the right [7].

To physically apply the AC bias to the modulator the following set up was used and is schematically shown in Figure 17. A 30-Mhz synthesized function generator (Stanford Research Systems, Model DS345) supplied a low-frequency square wave. This square wave was amplified by two amplifiers. Therefore, each amplifier produced half of the total voltage across the electrodes. One amplifier was a non-inverting high voltage amplifier and the other was an inverting high voltage amplifier. Each amplifier was supplied with high voltage from two DC power supplies (Kepco HP525M). One of the DC power supplies provided a negative voltage and the other DC power supply provided positive voltage for the bridge circuit amplifiers.

3-3 Data Addition

The ultimate goal of this project is to transmit an RF data signal. Therefore, to properly modulate the laser beam the polarity of the AC bias voltage must match the polarity of the RF data waveform [7]. Figure 19 shows how the polarity of the bias and data waveforms matches each other. When the AC bias voltage is applied, the voltage

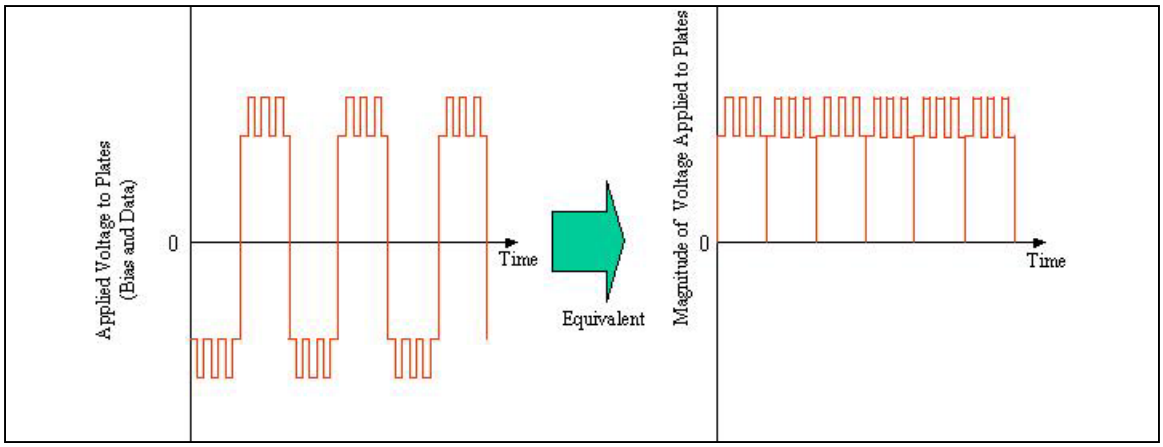

Figure 19. The bias and data waveforms must match in polarity to modulate correctly [7].

should be seen at the modulator, but filtered out of the signal portion of the circuit. The same can be said for the signal side of the circuit. The RF data signal should appear at the modulator, but should be filtered from reaching the bias side. The RF data signal was applied at the signal input, and is a generic sinusoidal wave that is created with a function generator (Stanford Research Systems, Model DS345). The sinusoidal wave is capable of being altered in frequency between 0 to 30-MHz and in amplitude from 0 to 10-V.

Greater than 10-V of RF drive amplitude was desired; therefore, a step-up transformer was built into the circuit shown in Figure 20. The step-up transformer is fabricated with an iron-core that has 4-turns in the primary and 20-turns in the secondary (1:5 ratio). Unfortunately this did not result in enough RF drive (8-V). The 10-V of RF drive amplitude never reaches the primary coil; rather an internal 50-ohm load lowers the voltage before reaching the primary coil. The number of windings in the primary coil and the iron-core was varied. Also, a matching coil was inserted into the circuit. In the end not enough gain was achieved to optimize the modulation. Although more RF drive

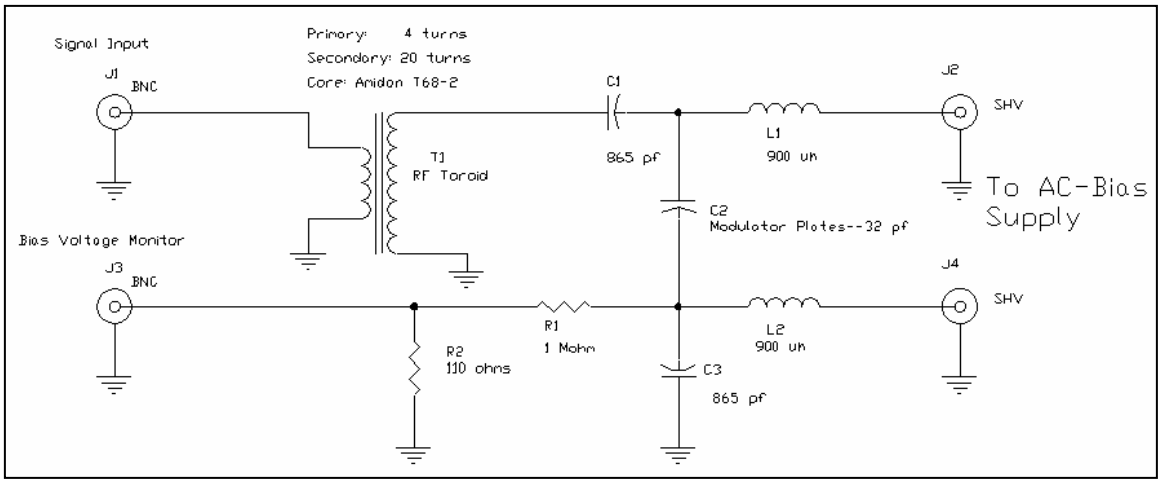

Figure 20. An electrical schematic of the modulator circuit. The AC-bias is supplied through the SHV connections. The RF data signal is input on the other side of the modulator through the BNC connection. Finally, the other BNC plug monitors the AC-bias voltage.

was desired it did not limit the RF signal from being transmitted. The fact that an RF signal was transmitted made the project a success. This circuit requires more research to obtain more drive and determine the optimum operating parameters for the modulator.

3-4 Experimental Arrangement

The laser beam was oriented perpendicularly to the modulator. Therefore, the beam was first directed off of a reflecting mirror to place the beam on the same optical axis as the modulator. From the reflecting mirror, the beam was sent through a lens to focus it into the proper size to form a match to the EH_{11} waveguide mode of the dielectric tube [7]. Once the beam passed through the modulator waveguide it was redirected with another reflecting mirror towards the detector placed on a different optical table. The detector was placed on a different optical table to give it distance from the RF signal created by the laser and modulator. Once the beam was sent from the second reflecting

mirror, it passed through a lens placed on the other optical beach to focus the beam into the detector. The detector was a liquid-nitrogen cooled mercury-cadium-telluride (HgCdTe) infrared detector. A picture of the experimental arrangement just described is depicted in Figure 21. Also, Figure 22 is a schematic that shows the path of the laser beam and the system to detect the RF signal and apply the AC bias.

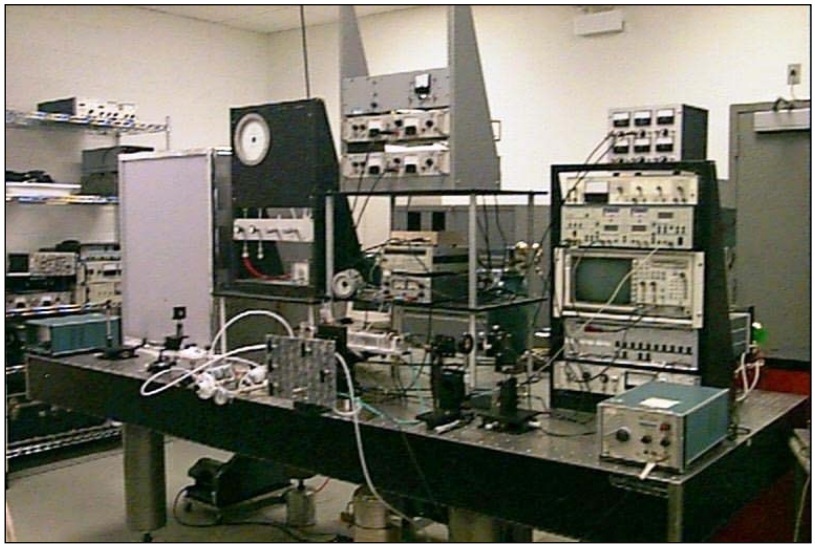

Figure 21. A picture of the experimental arrangement. The laser is located in its insulating housing on the left, with the modulator in the center, a detector near the right. Later the new detector was located on an adjacent optical table.

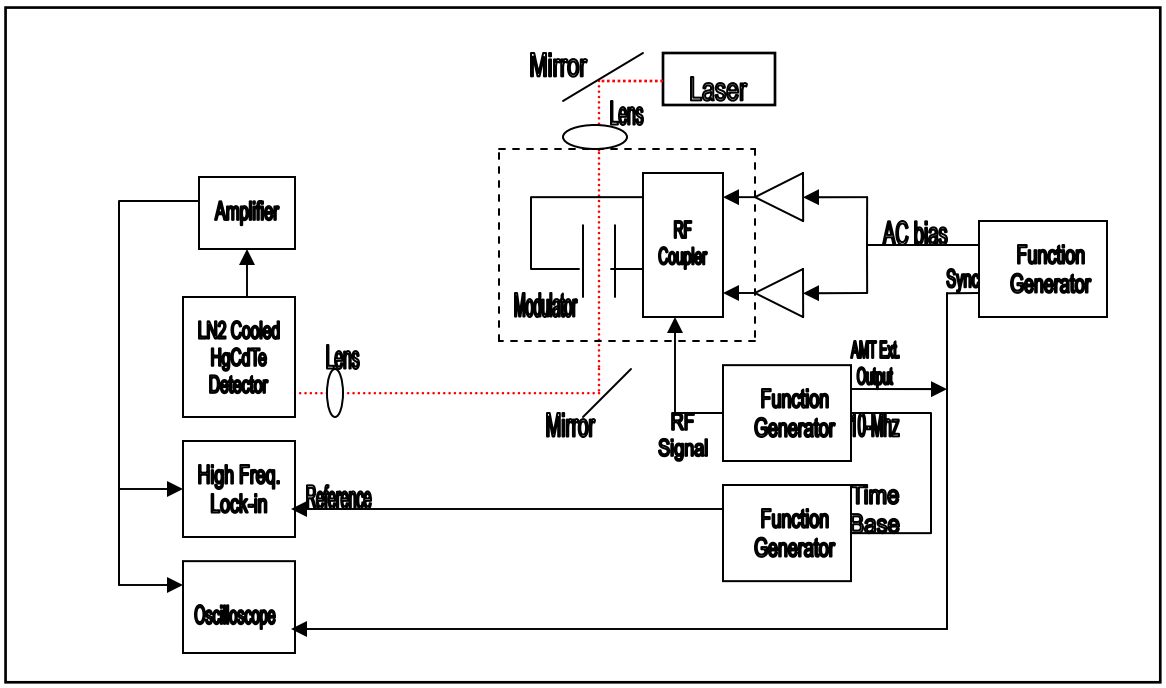

Figure 22. This is a schematic diagram of the experimental arrangement. Everything on the right is on one optical table. The equipment on the left was placed on an adjacent optical table. The dotted red line represents the laser beam. The components within the dotted lines are those shown in Figure 20.

Chapter 4:

Results

This thesis originally used a Stark-effect modulator constructed of ceramic measuring 36-cm long with an inner diameter of 0.9-mm. An attempt to characterize this modulator produced an electrical breakdown in the waveguide and prevented the development of sufficient voltage for modulation. Approximately 800-V were applied to the modulator, yet no Stark components were observed due to a breakdown in voltage at 600-V. The M = 4 and M = 3 peaks could not be observed as they were in the results produced by Hutchinson et al [7].

The ceramic waveguide was replaced with a borosilicate glass waveguide of the same length, but with a larger diameter. The inner- and outer- diameter of the new waveguide measured 1.8-mm and 3-mm, respectively. It was thought that the ceramic waveguide had many surface imperfections. Thus, this imperfection was a theory for the breakdown. Borosilicate glass should have a smoother surface than ceramic. A more perfect surface should create a more even electric field and should alleviate breakdown.

The larger diameter waveguide required a larger separation between the electrodes. A result of the greater electrode separation was a smaller electric field for a given applied voltage. Consequently, observations of the Stark components required larger applied voltage. Figure 23 represents the transmission versus applied voltage for this larger diameter cell, clearly showing that a larger voltage was required to observe the M = 4 component. This is a disadvantage of the larger diameter waveguide.

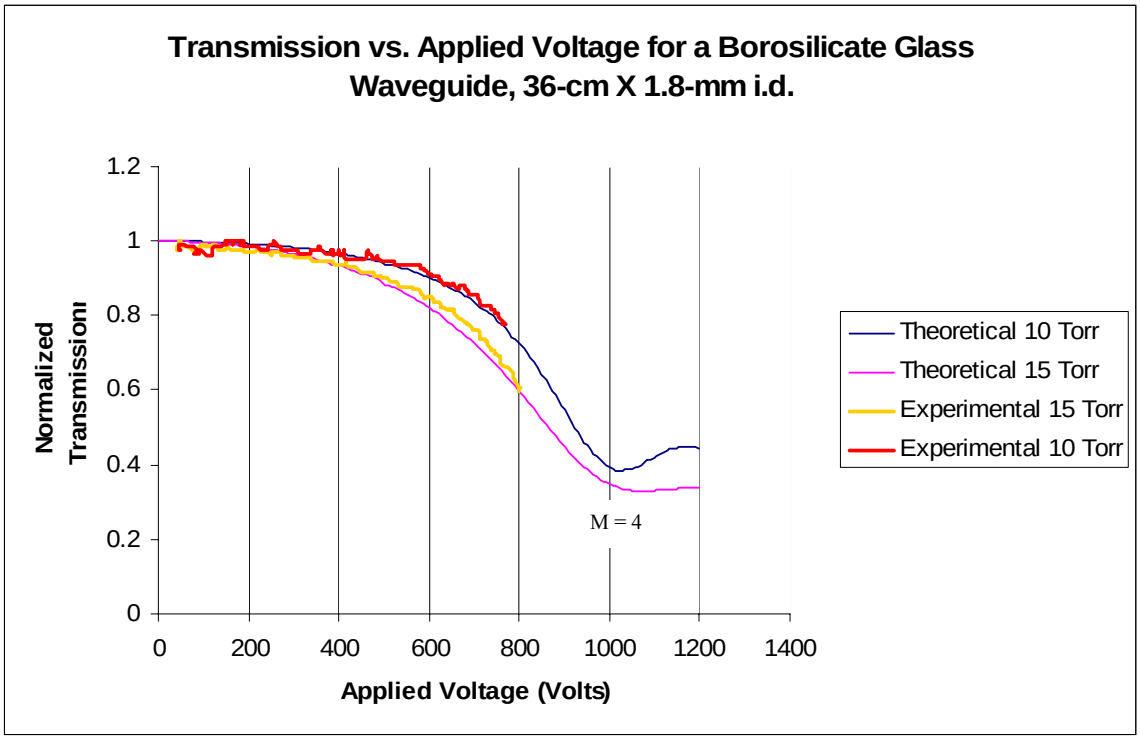

Figure 23. Normalized Transmission vs. Applied Voltage. There is good agreement between the theoretical model and experimental results.

The theoretical model was reevaluated for the new dielectric constant and diameter size of the waveguide. Also, the transmission at different applied voltages was recorded for the new design and compared to the model. This comparison characterized the modulator and is graphed in Figure 23. Figure 23 shows theoretical lines based on the model for 15-torr and 10-torr. The other two lines are based on experimental measurements. The measurements represent averaging experimental trials under the same modulator pressure. They show excellent correlation with the theoretical lines of their same pressure. The present bias voltage system does not allow for higher voltages to be reached. This is because the high voltage power operational amplifier (Apex PA94) has a high voltage output capability of ±400-V. A bridge circuit was used for the two

operational amplifiers. One was classified as inverting and the other non-inverting. Both were applied with -400-V and +400-V. This applied voltage results in a total availability of 800-V for the system. Figure 23 it appears has the M=4 peak occurring at 1000-V.

Although not enough applied voltage is available to reach the Stark components, it is not necessary to transmit data. A constant bias voltage between 700 to 800-V was applied to the electrodes based on the values observed in Figure 23. An area where the slope of the transmission line is steep is ideal for the CO_2 laser emission to transmit an RF data signal. If a bias voltage is chosen at a location along the transmission trend where the slope is not steep an RF data signal cannot be transmitted as well. This fact is represented with the aid of the transmission curve shown in Figure 24. Figure 24 was created with the model at 15-torr of NH_2D. The trend described as the "drive," represents an RF sinusoidal signal applied to the modulator. Essentially this is a generic data signal to test the system. The peak-to-peak voltage of the drive was 8-V. When it contacts the transmission curve it is transmitted by the modulator. Because the peak-to-peak voltage of the drive was small, a very weak signal is transmitted. Ideally, a much larger peak-to-peak drive voltage is desired to optimize modulation. Unfortunately the step-up transformer shown in Figure 20 was not able to amplify the drive signal better. A drive voltage of approximately 100-V peak-to-peak would be more ideal for this modulator. Therefore, this needs more investigating. The thesis is still considered a success. The goal was to transmit an RF signal and this was accomplished.

The transmitted RF signal is depicted in Figures 25 and 26. This signal was detected with a liquid-nitrogen HgCdTe detector. This sensitive detector was required because the RF drive voltage was small. Also, an analog oscilloscope was used instead

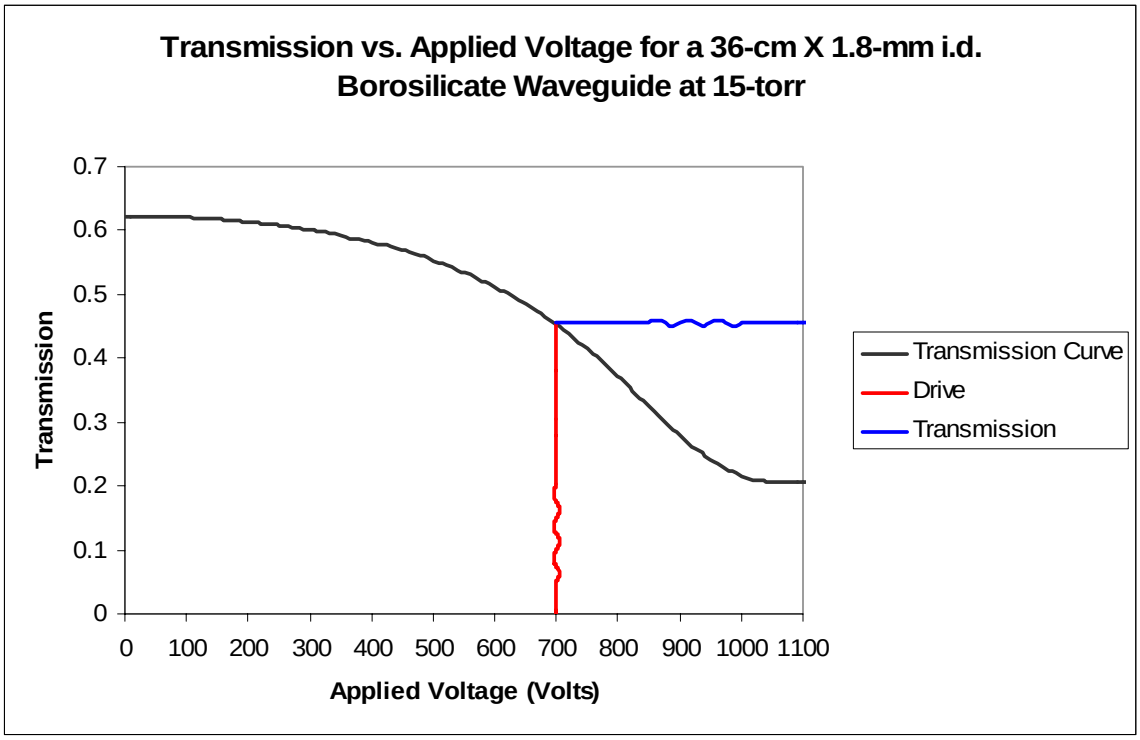

Figure 24. The RF drive signal had 8-Vpp driven to the modulator. This resulted in a small RF transmission signal. The red curve is the 8-Vpp of sinusoidal RF drive applied to the modulator. When it contacts the transmission curve it is carried to the detector by the CO_2 laser. The transmitted curve is represented by the blue trend.

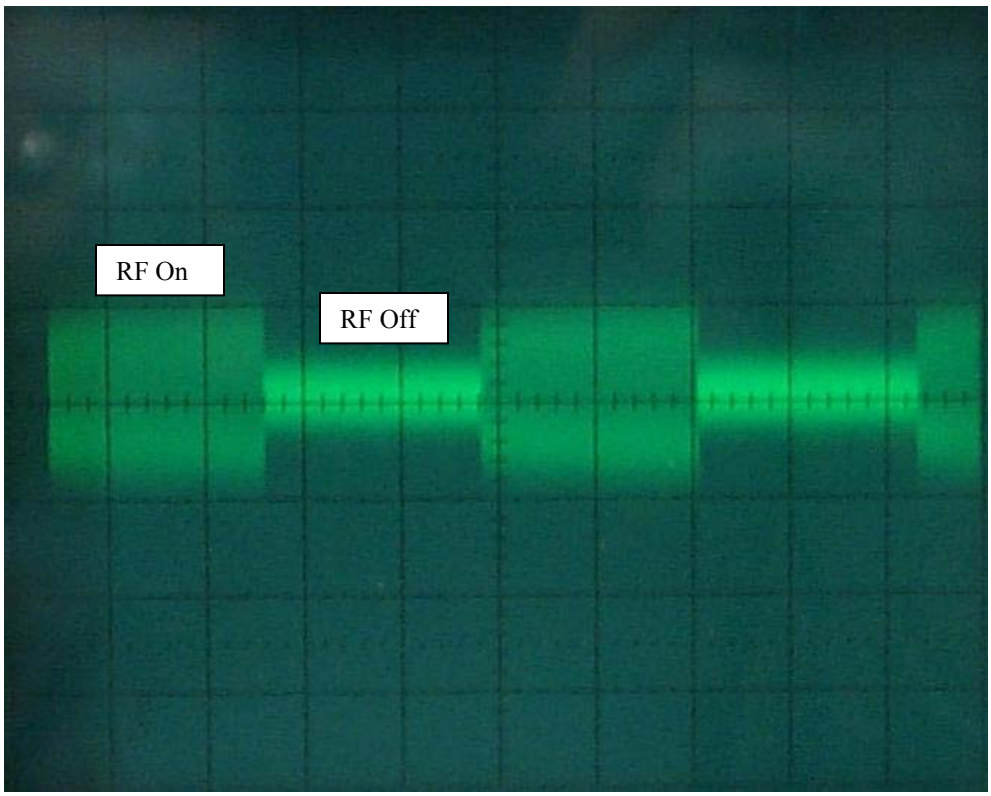

Figure 25. This is the detected RF transmission. The horizontal scale is 0.2-ms/division, while the vertical scale is 10-mV/division. The area labeled as "RF On" represents the area where the detector has detected RF signal. The "RF Off" region has no signal. The background signal in the "RF Off" region is due to interference from other sources such as the RF excitation of the CO_2 laser. The RF was turned off by modulating the RF function generator source with the AC bias function generator.

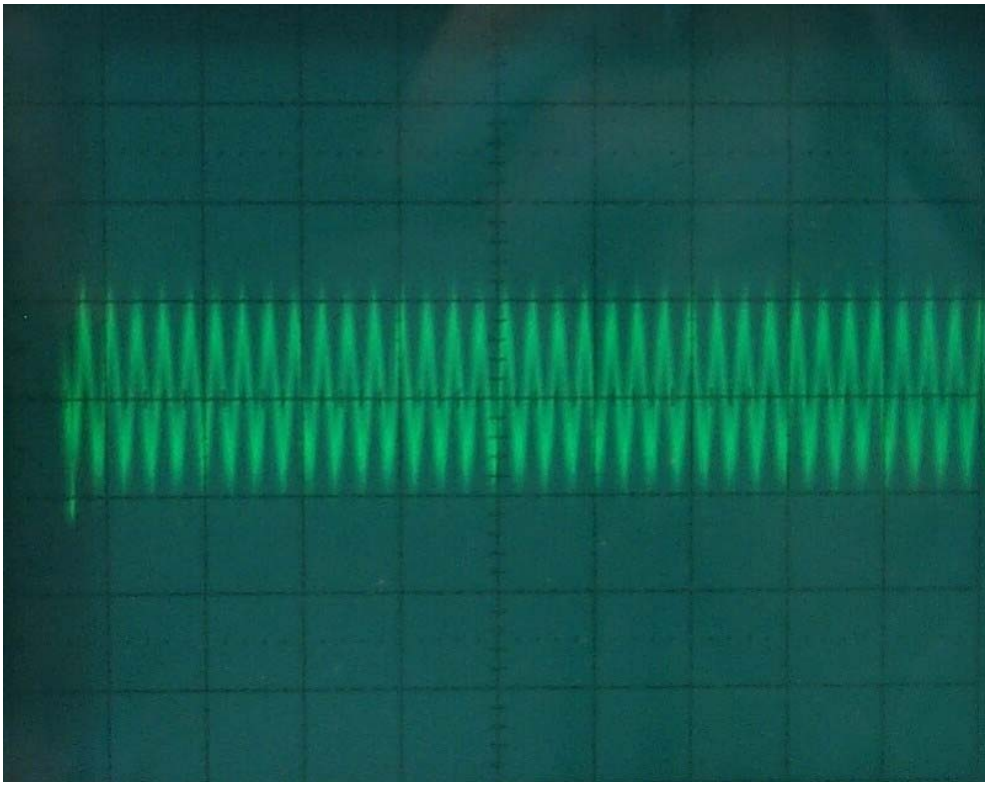

Figure 26. This shows the transmitted RF sinusoidal signal. The horizontal scale is 200-ns/division, while the vertical scale is 10-mV/division. This view of the transmitted signal is a "zoomed in" version of the "RF On" region of Figure 25, with an expanded horizontal scale. It clearly shows the RF sinusoidal signal was successfully transmitted.

of a digital oscilloscope. The available digital oscilloscope did not have sufficient sensitivity to reliably display the small RF transmission signal. The analog oscilloscope was able to highlight the small RF transmission signal. The analog oscilloscope was satisfactory for viewing the signal; however, more accurate analysis could have been obtained with the measurement capabilities of a digital oscilloscope. A high frequency lock-in amplifier was used to measure the transmitted RF signal amplitude, with a digital meter connected to its output to make quantitative measurements of the transmission signal.

Figure 25 has regions labeled "RF On" and areas labeled RF Off." The area labeled "RF On" is the transmitted RF sinusoidal signal. Figure 26 shows the "RF On" region "zoomed" into. When zoomed into, the transmitted RF sinusoidal signal can be clearly observed. This provides excellent evidence that the modulator functions since the transmitted and detected RF frequency and amplitude is observed to be closely correlated with that used to drive the modulator. Figure 25 also has regions labeled "RF Off." Here the function generator supplying the RF drive was modulated with the function generator supplying the AC bias signal. The reason for the "RF Off" was to eliminate the switching transients created by the AC biasing. It appears that a background signal is measured at the "RF Off" region in Figure 25. This background was confirmed to be RF interference that may have developed from the 60-MHz RF used to excite the CO_2 laser.

Three separate measurements of the transmitted RF sinusoidal signal were taken under the conditions described above. Under these conditions, the optimum drive frequency was determined to be 16.4 MHz. This was true for all reasonable operating pressures.

A second measurement surveyed for saturation of the transmitted signal. Consequently, the peak-to-peak voltage of the RF drive signal was varied and the amplitude of the received signal was observed. The result is given in Figure 27. Here, as the voltage of the drive is increased, the amplitude of the received signal also increases. The saturation is dependent on the transmission curve slope, shown in Figure 24. Thus, this would be a more interesting measurement with large RF drive because it would cause the slope to vary more.

Finally, the transmitted RF signal amplitude was measured as a function of modulator pressure. This was studied to determine the optimum operating pressure, and to compare with theory (see appendix for calculation). The theory is based on a quantity called the figure of merit. The figure of merit is the modulation index multiplied by the average transmission signal. The modulation index divides the difference of the transmission signal by the difference of drive signal. Figure 28 compares the theoretical model for the figure of merit to the experimental results of the figure of merit, as a function of modulator pressure. The most obvious result is that the experimental results are shifted to the right with respect to the model. According to the model the optimum operating pressure is 9-torr, while the experimental trend displays an optimum at 12-torr. This requires further investigation, but there is a possible explanation. It may be that the modulator requires higher drive voltages to accurately reproduce the pressure-dependence exhibited by the model in Figure 28. Nevertheless, the trends shown in that figure are similar in their behavior.

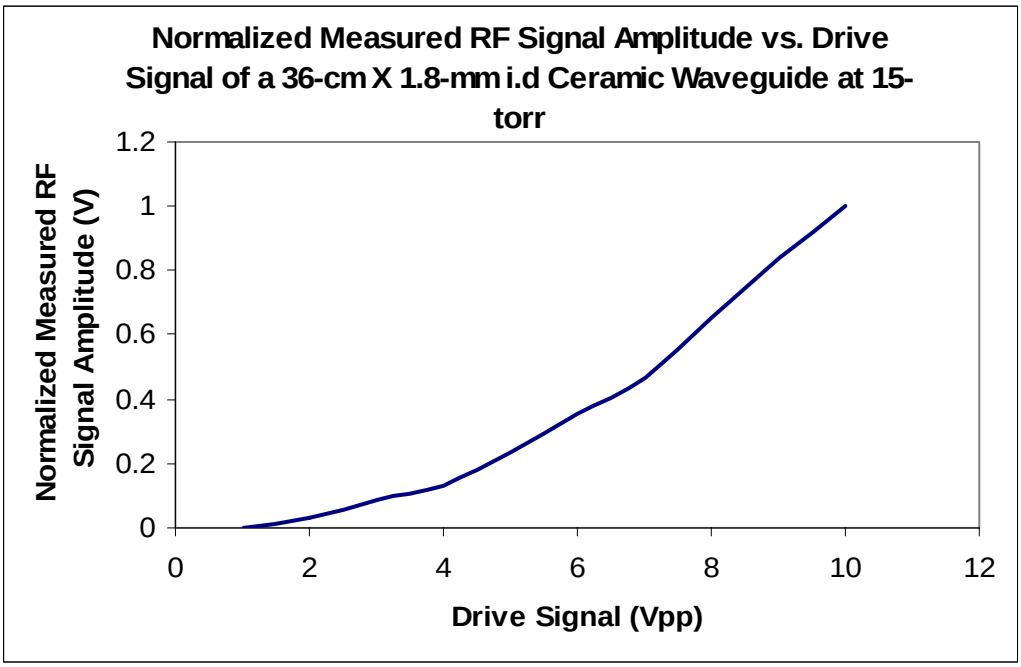

Figure 27. Normalized Measured RF Signal Amplitude vs. Drive Signal. The Measured RF Signal Amplitude was normalized to the largest measured amplitude. This verifies that along the transmission curve, shown in Figure 24, no saturation was measured.

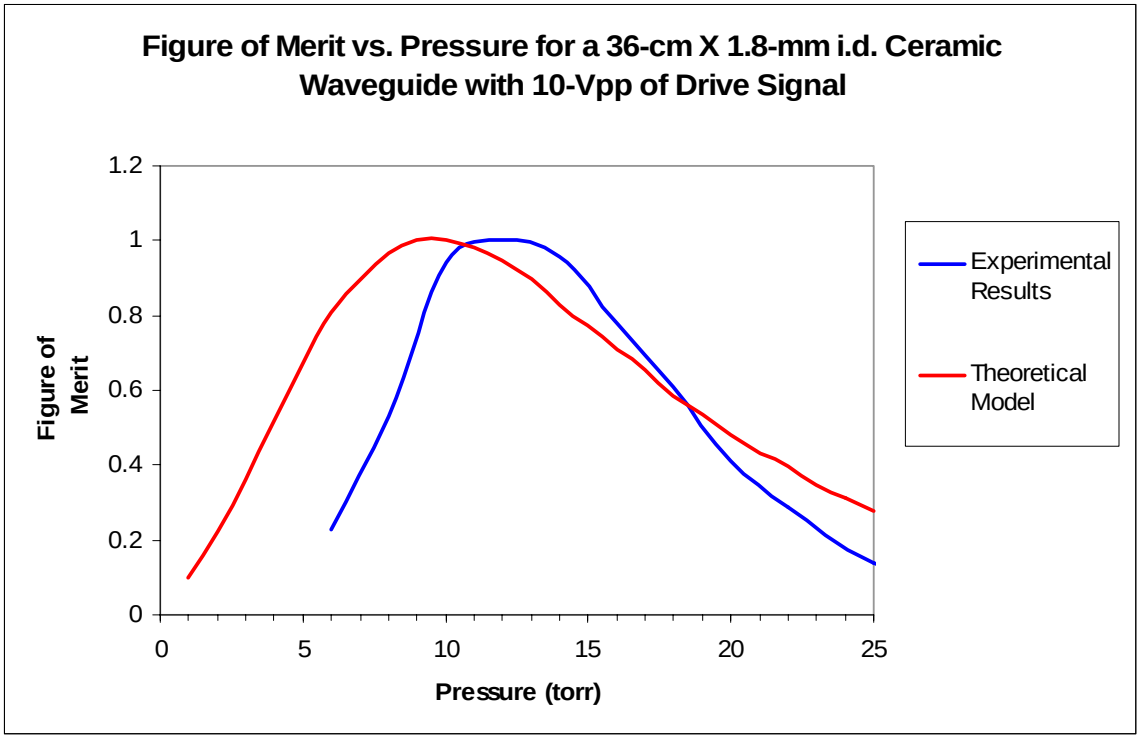

Figure 28. Figure of Merit vs. Pressure. According to the theory the optimum operating pressure is 9-torr for NH_2D. The experimental result points to an optimum pressure of 12-torr of NH_2D.

Chapter 5:

Conclusion

Prior to this thesis, Hutchinson et al. [7] had characterized the DC performance of a Stark-effect modulator. Their characterization was for a Stark-effect modulator with a borosilicate waveguide that measured 20-cm long and had an inner diameter of 0.9-mm. This thesis used a Stark-effect modulator with a borosilicate waveguide that measured 36-cm long and had an inner diameter of 1.8-mm. This increased length allows for greater modulation amplitude. The goal of this thesis was to transmit an RF data signal for the first time. Before an RF signal could be transmitted, the new Stark-effect modulator had to be characterized. The Stark-effect modulator was successfully characterized. The characterization was considered a success because it matches the predicted model. The match of the model and the experimental results are graphed in Figure 23. This experiment offers confidence that the theory is understood.

According to the characterization of this particular Stark-effect modulator, approximately 600- to 1000-V of total applied bias voltage to the modulator should be sufficient to transmit data. At an applied voltage of 700-V an RF sinusoidal signal was transmitted. An applied voltage of 700-V was used because 800-V was the maximum capability of the available AC bias system. The transmitted RF signal was successfully detected by a receiver. This result provides a prototype for a future LWIR free-space communication link.

The RF modulator drive signal had 8-V peak-to-peak voltage. This small drive voltage resulted in a small RF transmission signal. Therefore, a sensitive liquid nitrogen cooled HgCdTe detector was required to detect the RF signal. A method to increase the drive signal needs to be developed for a better prototype. Hopefully this will be solved in the future.

Measurements of the RF transmission signal amplitude were taken. First, it was verified that saturation of the transmitted signal did not occur as the RF drive signal was increased. Rather, the transmitted RF signal increased as the RF drive amplitude was increased. Saturation could be present with a larger RF drive signal, since applied saturation is dependent on the transmission curve slope.

Next, the greatest transmitted RF signal amplitude results from a modulation frequency of 16.4-MHz. The transmitted RF signal drops in magnitude at both higher and lower frequencies. This only holds true for the current circuit arrangement. By altering the step-up transformer shown in Figure 20, the optimum frequency can be changed.

Finally, the RF signal transmission was optimized with a modulator pressure of 12-torr, according to the experimental values. This was not confirmed by the model, which predicts that the maximum transmission should occur at 9-torr of NH_2D. While the peak values are different, the trends are the same, only shifted from each other.

While more optimization is clearly required before the modulator may be integrated into a LWIR free-space communication link, the work of this thesis has been successful in demonstrating that the dielectric Stark-effect modulator is capable of transmitting data at RF bit-rates.

Besides optimizing the pressure and RF drive signal, the molecular gas and laser line may be optimized. There are potentially many more ammonia isotopes and CO_2 laser isotopes to experiment with. The best combinations of lasing and absorption transitions need to be identified. Thus far only two transitions have been identified in literature and from this thesis. The reason to study this is to determine which combination may result in the lowest drive voltage. A lower drive voltage could result in higher speed operation. The goal of the future LWIR free-space communication link is 2.5-Gbits/sec over a range of >6 kilometers. Thus, the best transition of ammonia and CO_2 needs to be found.

References

[1] C.K. Asawa and T.K. Plant, "Wideband modulation of the $C^{13}O_2^{16}$ laser R(18) line at 10.784 μm with an $N^{14}H_3$ Stark Cell," *Appl. Phys. Lett.*, vol 30, no 2, January 15, 1977, pp 96-98.

[2] R.G. Brewer, M.J. Kelly, and A. Javan, "Precision Infrared Stark Spectra of $N^{14}H_2D$ Using Lamb Dip," *Phys. Rev. Lett.*, vol 23, no 11, September 15 1969, pp. 559-563.

[3] P.C. Claspy and Y.H. Pao, "Basic Characteristics of High-Frequency Stark-Effect Modulation of CO_2 Lasers," *IEEE J. Quantum Electronics*, vol QE-7, no 11, November 1971, pp. 512-519.

[4] H.O. Granberg, "Wideband RF Power Amplifier," Motorola Semiconductor Products.

[5] HITRAN, Molecular Line Database, U.S. Air Force, 1996.

[6] D.P. Hutchinson, R.K. Richards, M.D. Chidley, and J.T. Simpson, "All Weather Long-Wavelength Infrared Free Space Optical Link for FCS vehicle to vehicle Communications," *23rd army science conference,* Orlando, fl, Dec 2-5, 2002.

[7] D.P. Hutchinson, R.K. Richards, J.T. Simpson, M.L. Simpson, "All Weather Long-Wavelength Infrared Free Space Optical Communications," *SPIE,* vol 4821, pg 44-49.

[8] A.R. Johnston and R.D.S. Melville, Jr., "Stark-Effect Modulation of a CO_2 Laser by NH_2D," *Appl. Phys. Lett.*, vol 19, no 12, December 15 1971, pp. 503-506.

[9] R. Karplus, "Frequency Modulation in Microwave Spectroscopy," *Phys. Rev.*, vol.73, no 9, May 1, 1948, pp. 1027-1034.

[10] A. Landman, H. Marantz, and V. Early, "Light Modulation by Means of the Stark Effect in Molecular Gases-Application to CO_2 Lasers," *Appl. Phys Lett.*, vol 15, no 11, December 1, 1969, pp. 357-360.

[11] B.P. Lathi, *"Signal Processing and Linear Systems,"* (Berkeley Cambridge Press, Carmichael, CA, 1998).

[12] F.L. Pedrotti, S.J. and L.S. Pedrotti, *"Introduction to Optics,"* (Prentice Hall, Upper Saddle River, NJ, 1993).

[13] T.K. Plant and R.L. Abrams, "Broadening and absorption coefficients in $N^{14}H_2D$," *Appl. Phys.*, vol 47, no 9, September 9, 1976, pp. 4006-4008.

[14] F. Shimizu, "Stark Spectroscopy of NH_3 ν_2 Band by 10-μ CO_2 and N_2O Lasers," *Chem. Phys*, vol 52, no 7, April 1, 1970, pp. 3572-3576.

[15] C.H. Towes and A.L. Schawlow, *"Microwave Spectroscopy,"* (McGraw-Hill, New York, 1955).

[16] C.J. Walsh, "An RF excited circular waveguide CO2 laser," Rev. Sci. Instrum., Vol 61, no 9, Sept. 1990.

Appendix

Multiple M-Level Contributions for a Stark Modulator

Electrode Spacing. $dia := 0.356\,cm$

Cell Length. $l := 35.56\,cm$

Doppler Width. $bd := 82\,MHz$

Electric field required to offset absorption to laser line center. $Eo := 3800\,\frac{V}{cm}$

Non-electrified beam region in modulator. $lfree := 15.96\,cm$

Pressure Broadening Coefficient. $C := 32 \cdot 10^{6} \cdot \frac{Hz}{torr}$

Fraction of NH_2D. $\kappa := .44$

From e-field modeling. $efactor := 1.3579$

Frequency offset of laser line center. $\varepsilon 0 := 2189 \cdot MHz$

Absorption Coefficient. $\gamma H := 0.05\,cm^{-1}$

Math counter to calculate curve. $i := 1 .. 120$

Operating pressure in cell. $P_k := k\,torr$

$k := 1 .. 25$

M - Level Dependent Stark Shift. $S_j := 0.568\,10^{6} \cdot \frac{j-4}{4} \cdot \frac{Hz \cdot cm}{V}$

$j := 0 .. 8$

Applied voltage. $V_i := 10 \cdot i \cdot V$

Equations for the Transmission Curve From Johnston and Melville

$$Ein_i := \frac{efactor}{3.56} \cdot V_i \cdot mm^{-1}$$

$$\varepsilon(j,i) := \varepsilon 0 - S_j \cdot Ein_i$$

$$b1_k := \sqrt{bd^2 + \left(C \cdot P_k\right)^2}$$

$$\gamma(k) := \sum_j \frac{\left(\gamma H \cdot C \cdot \kappa \cdot P_k \cdot b1_k\right)}{\varepsilon 0^2 + \left(b1_k\right)^2}$$

$$\gamma 1_{i,k} := \left[\sum_j \frac{\left(\gamma H \cdot C \cdot \kappa \cdot P_k \cdot b1_k\right)}{\varepsilon(j,i)^2 + \left(b1_k\right)^2}\right]$$

$$trans1(i,k) := 1 \cdot e^{-\gamma 1_{i,k} \cdot l - \gamma_k \cdot lfree}$$

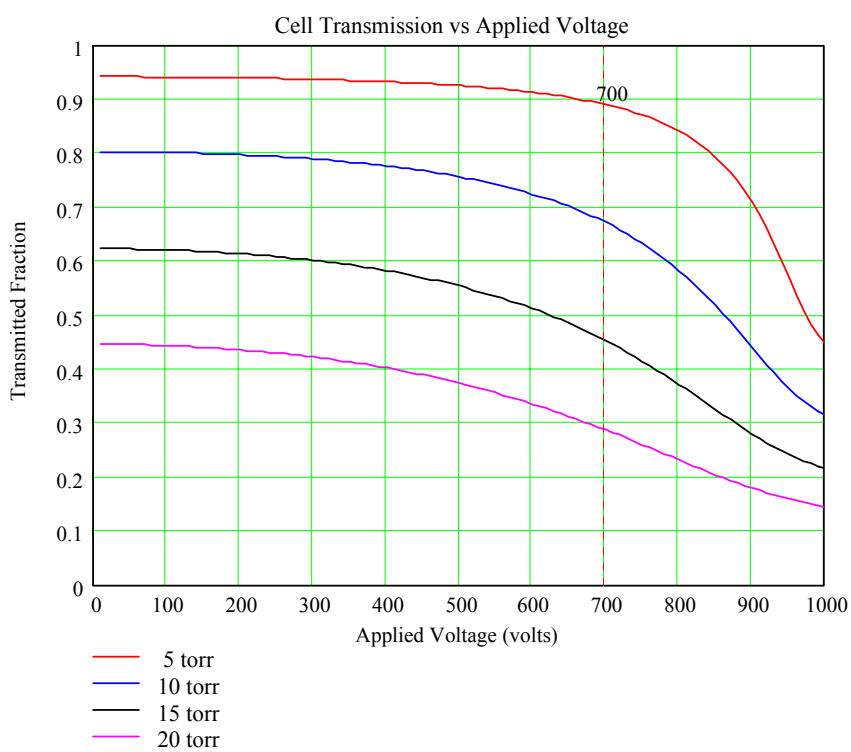

Modulation Index

$$\text{modindex75}(k) := \frac{(\text{trans1}(73,k) - \text{trans1}(81,k))}{\text{trans1}(73,k) + \text{trans1}(81,k)}$$

$$\text{modindex100}(k) := \frac{(\text{trans1}(75,k) - \text{trans1}(85,k))}{\text{trans1}(75,k) + \text{trans1}(85,k)}$$

$$\text{modindex150}(k) := \frac{(\text{trans1}(69,k) - \text{trans1}(85,k))}{\text{trans1}(69,k) + \text{trans1}(85,k)}$$

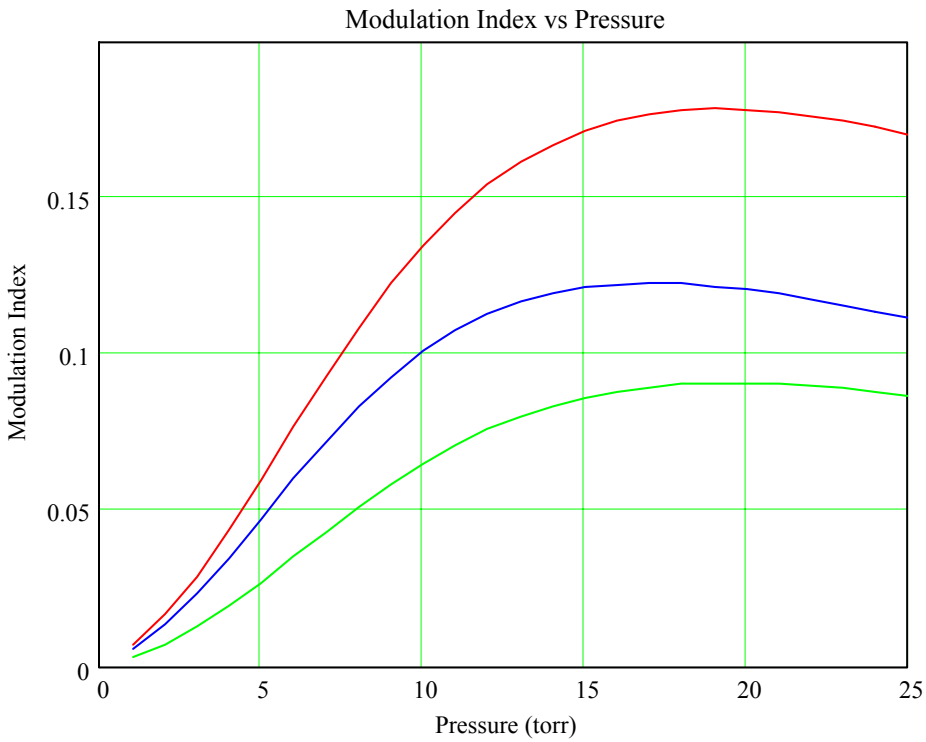

Figure of Merit

$$mod75_k := modindex75(k) \cdot \frac{(trans1(73,k) + trans1(81,k))}{2}$$

$$mod100_k := modindex100(k) \cdot \frac{(trans1(75,k) + trans1(85,k))}{2}$$

$$mod150_k := modindex150(k) \cdot \frac{(trans1(69,k) + trans1(85,k))}{2}$$

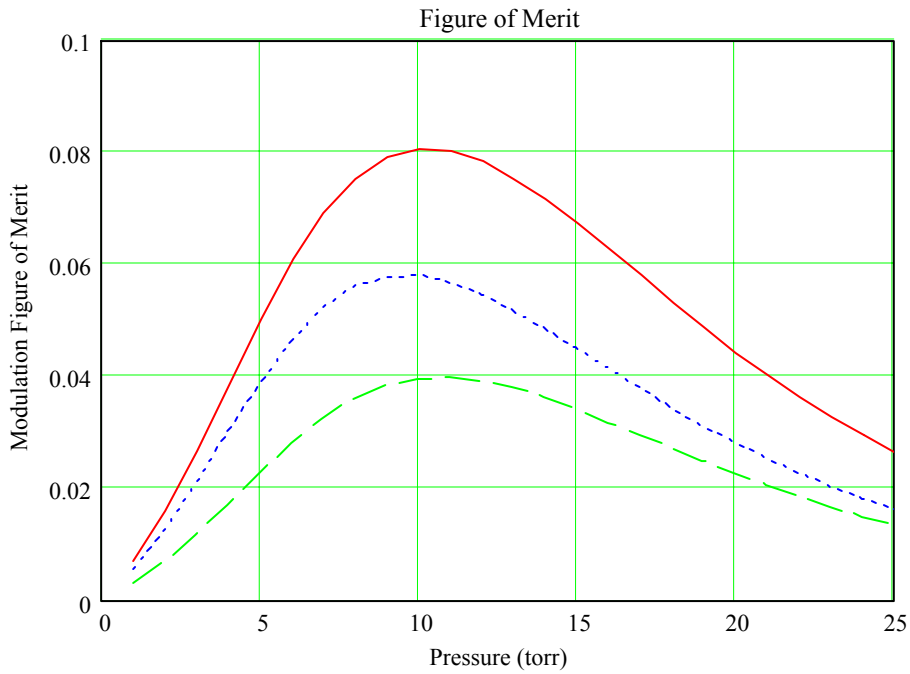

Vita

Ryan Lane Holloman was born in Albuquerque, New Mexico, on November 22, 1979 to Charles and Pamela Holloman. He was raised in Westminster, Colorado, and graduated from Standley Lake High School in 1998. He received a Bachelor of Arts in physics from the University of Northern Colorado in 2002. While an undergraduate, he participated in two National Science Foundations sponsored Research Experience for Undergraduates (REU) programs. The first appointment was at Kansas State University, during the summer of 2000. While there, Ryan worked in experimental atomic physics trapping Rubidium atoms with a Magneto-Optical Trap (MOT). During the summer of 2001, Ryan attended the University of Massachusetts Lowell. There he worked in health physics, characterizing the response of UML's stack monitor system designed for their 1 MW research reactor. In 2005 Ryan received his Master of Science degree in physics from the University of Tennessee, and performed his thesis research at the Oak Ridge National Laboratory.